Mechanical activation of TWIK-related potassium channel by nanoscopic movement and rapid second messenger signaling.

E. Nicholas Petersen[1,4], Mahmud Arif Pavel[1], Samuel S. Hansen[1], Manasa Gudheti[5], Hao Wang[1,4], Zixuan Yuan[1,4], Keith R. Murphy[2,3], William W. Ja[2,3], Heather A Ferris[5], Erik M. Jorgensen[6], Scott B. Hansen[1]

[1]Departments of Molecular Medicine, [2]Department of Neuroscience, [3]Center on Aging, [4]Scripps Research Skaggs Graduate School of Chemical and Biological Science, The Scripps Research Institute, Scripps, Florida 33458, USA

[5]Division of Endocrinology and Metabolism, [5]Center for Brain Immunology and Glia, Department of Neuroscience, University of Virginia, Charlottesville, VA 22908, USA

[6]Department of Biology, Howard Hughes Medical Institute, University of Utah, Salt Lake City, UT 84112, USA

*Correspondence: shansen@scripps.edu

Summary: Shear thinning activates TREK-1 through a second messenger.

Abstract

Rapid transduction of force into a biological signal allows living cells to respond to mechanical changes in their environment. Force is thought to first act on the plasma membrane and alter membrane associated proteins. The enzyme phospholipase D2 (PLD2) is mechanosensitive and associates with the membrane through a covalently attached palmitate lipid (palmitoylation) and its affinity for a structured membrane-lipid site comprised of cholesterol and saturated ganglioside (GM1). Here we show stretch activation of TWIK-related K^+ channel (TREK-1) is mechanically activated by movement from ordered GM1 clusters to 4,5-bisphosphate (PIP_2) clusters. First, force (shear or stretch) deforms the ordered GM1 lipids and lowers cholesterol in the membrane. Second the deformation disrupts the interaction of palmitate with the ordered GM1 lipids allowing a complex of TREK-1 and PLD2 to move to PIP_2 clusters where the enzyme produces the second messenger phosphatidic acid (PA) that helps gate the channel. Co-expression of catalytically dead PLD2, devoid of PA production, inhibits TREK-1 stretch currents in the cell membrane. Loading cultured cells with cholesterol clusters TREK-1 with GM1 lipids and inhibits the channel and depletion of cholesterol in astrocytes moves TREK-1 away from GM1. Reduction or elimination of PLD2 expression in flies results in hypersensitivity to mechanical force—decreased thresholds. We conclude the ordered lipids sense force and PLD2 combines with TREK-1 to elicit a mechanical response. The hypersensitivity of PLD2 deficient flies suggests an *in vivo* role for PA lipid signaling in setting mechanosensitivity and pain thresholds.

Keywords: lipid raft; signaling lipid; phospholipase D; mechanosensation; shear thinning

Introduction

All cells respond to force (mechanosensation)[1–3]. Mechanosensation requires both sensing and transducing the force. Ion channels are important meditators of force. Some ion channels are downstream of multi-step signaling cascades[4]. For example, transient receptor potential (TRP) channels are activated by multi-step mechanical signaling cascades[5,6] including those involving mechanosensitive G-protein coupled receptors (GPCRs)[4,7–10].

TWIK-related K^+ channel subtype 1 (TREK-1) is an analgesic mechanosensitive channel of the two-pore-domain potassium (K2P) family that inhibits neuronal firing and reduces pain by the release of potassium[11]. Interestingly, the enzyme phospholipase D2 (PLD2) binds directly to the C-terminus of TREK-1 and activates the channel through local production of phosphatidic acid[12]. PLD2 is also mechanosensitive[13,14]. Shear of 3 dynes/cm^2 robustly increases PLD2 catalytic activity[13]. PLD2 is palmitoylated at cysteines near its pleckstrin homology (PH) domain, which at rest causes PLD2 to bind to a specific site comprised of monosialotetrahexosylganglioside (GM1) lipids and cholesterol in the liquid ordered (L_o) region of the membrane[15,16] (Supplemental Fig. S1a-b). The PH domain also binds phosphatidylinositol 4,5-bisphosphate (PIP_2) which opposes association with GM1 lipids by trafficking the enzyme to the liquid disordered (L_d) region of the membrane[13] where it is activated by substrate presentation[17] (Supplemental Fig. S1c).

PLD2 mechanosensitivity and TREK-1 binding raises several important questions: first, does PLD2's mechano-sensitivity contribute to mechanosensitivity of TREK-1 channels? The TREK-1 C-terminus that binds PLD2 is also required for TREK-1 mechanosensitivity in cellular membranes[18–20] and the same C-terminal segment is required for PLD2 dependent anesthetic sensitivity of the channel[14]. Lastly, how does PLD2 sense mechanical force on the membrane when it has only a lipid palmitate to associate with the membrane, i.e., no transmembrane domain? Here we show mechanical activation of TREK-1 in cultured cells includes mechanically induced movement of TREK-1 and the production of PA by PLD2.

Results

PLD2 dependent TREK-1 activation.

To test the contribution of PLD2 to the mechanical sensitivity of TREK-1, we measured pressure currents with and without a catalytically dead K758R PLD2 mutant (xPLD2)[21] in HEK293 cells. We used HEK293 since they have very little endogenous potassium currents and by over expressing the channel, we can attribute the measured current to TREK-1. Expression of TREK-1 was monitored by an eGFP tag on the c-terminus. All constructs expressed well and could be seen on the surface of the cell (Fig. S2a-b). We expected TREK-1 to be less sensitive to mechanical activation with xPLD2 (i.e., xPLD2 should reduce PLD2 dependent activation of TREK-1).

We found overexpression of xPLD2 inhibited a significant portion of the stretch-activated TREK-1 current (Fig. 1a-c) in cultured HEK293T cells. Currents, measured in the inside out configuration with negative pressure (from 0 to -60 mmHg) decreased >80% from 0.181 ± 0.04 to 0.035 ± 0.013 pA/μm^2.Truncating the C-terminus to remove the putative PLD binding site (Fig. S3a) decreased the TREK-1 pressure current > 85% to 0.025 ± 0.013 pA/μm^2 (Fig. 1c and Fig. S3b).

Previous work showed purified reconstituted TREK-1 is directly sensitive to force absent PLD2[22,23]. To characterize the PLD2 independent (i.e., direct) component of TREK-1 mechanosensitivity in a cellular membrane (mammalian lipids), we compared cells expressing the truncated TREK1 (TREK-1 trunc) with mock transfected HEK293T cells (no TREK-1). We found TREK-1 trunc had 0.046 ± 0.023 pA/μm^2 more current (p=0.08) (Fig. 1c inset). Similarly in cells expressing xPLD2 with full length TREK-1, the channel showed a small, 0.060 ± 0.035 pA/μm^2 increase in currents (p=0.11). This PLD2 independent current is consisted with direct TREK-1 mechanosensitivity seen in liposomes.

As a control, to confirm surface expression and function of TREK-1 in the presence of xPLD2, we measured TREK-1 basal resting currents at 0 mV with and without xPLD2 (Fig. 1d). TREK-1 is a potassium leak channel with basal currents in cultured cells[12]. Consistent with previous studies, we found significant TREK-1 basal current with (24.0 ± 4.2 pA/pF) and without (16.9 ± 4.3 pA/pF) xPLD2 [12]. Currents from FL TREK-1 with xPLD2 was significantly higher than a control, C321 truncation of TREK-1, which we found to have no current. This result suggests that FL TREK-1 is expressed and functional in the presence of xPLD2.

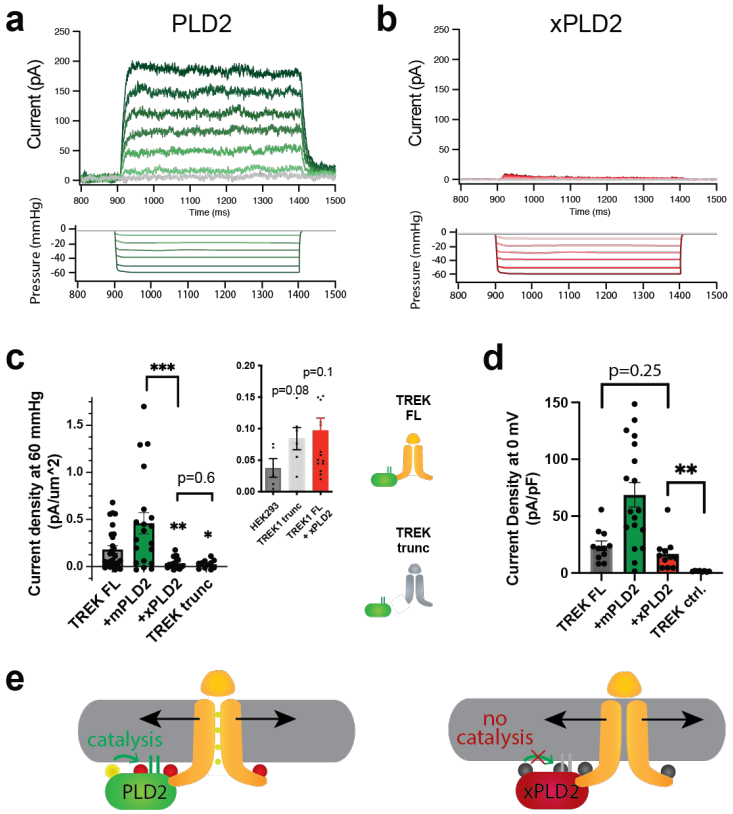

Figure 1. **PLD2 dependent mechanical activation of TREK-1 channels.** (**a-b**) Representative traces from pulled patches of human TREK-1 over expressed in HEK293T cells with phospholipase D2 (PLD2, green traces) (**a**) or catalytically dead PLD2 (xPLD2, red) (**b**) with pressure clamp (0-60 mmHg at +30 mV). (**c**) The data, minus HEK293 background (0.04 ± 0.02 pA/μm^2 n=5 (inset)), are summarized for -60 mmHg. Compared to endogenous PLD2, the expression of xPLD2 eliminated the majority of detectible TREK-1 pressure current (p<0.007, n=16-23), as did a truncated TREK-1 (TREK1 trunc) lacking the PLD2 binding site (p=0.002, n=15-23) The inset compares mock transfected HEK293T cells with TREK-1 trunc and full length (FL) TREK1 + xPLD2, indicative of direct TREK-1 activation. Astricts are relative to TREK1 FL except where noted by a bar. (**d**) Whole cell TREK-1 potassium currents with and without xPLD2. TREK-1 is expressed and functional in the presence of xPLD2. TREK-1 control (ctrl) is a C-terminal truncation (C321) of TREK-1 found to have very little current. (**e**) Cartoon showing PLD2 dependent TREK-1 opening. TREK-1 senses force causing the channel to favor an open conformation (black arrows). When PLD is active it makes phosphatidic acid (PA) which maintains the open state. If PA is not present the channel is not maintained in the open state.

Furthermore, this result shows that the pressure current (Fig. 1c) is much more sensitive to xPLD2 than the leak current (Fig. 1d; TREK FL, grey bar vs. +xPLD2, red bar)

Further establishing a role for PLD2 in TREK-1 mechanical activation, overexpression of TREK-1 with endogenous or over-expressed levels of wild type (WT) mouse PLD2 (mPLD2) led to a robust TREK-1 pressure-dependent current in HEK 293 cells (Fig. 1a, see Supplemental Fig. S3b for raw traces). The relative xPLD2 inhibition was highly significant compared to TREK-1 with or without overexpression of mPLD2 (p<0.002 and 0.007 respectively, Fig. 1c).

The PLD dependent threshold from TREK-1 was relatively sensitive, responding to negative pressure (0 to -60 mmHg) with a half maximal pressure (P_{50}) of ~32 mmHg and yielding up to 200 pA of TREK-1 current (Fig. 1a and Supplemental Fig. S3c) consistent with previous studies[19,22].

Mechanical activation of TREK-1 by movement between nanodomains.

As mentioned, fluid shear causes PLD2 to move from cholesterol dependent GM1 clusters to PIP_2 clusters and this activated the enzyme (Fig. S1)[13]. Since TREK-1 binds to PLD2 we reasoned the channel could be similarly mechanically activated by a movement from GM1 to PIP_2 lipids. To directly visualize TREK-1 in sheared lipids, we developed a procedure to chemically fix membranes during shear (Fig. 2a). Cultured HEK293T cells expressing TREK-1 and mPLD (identical to our electrophysiology experiments) were sheared at 3 dynes/cm^2 (a physiologically relevant force to cells[13,24]), fixed and labeled for two-color dSTORM. For TREK-1 protein labeling, we used the direct self-blinking properties of the eGFP tag. For labeling lipids, we used Alexa 647 (A647) anti-PIP_2 antibody or A647 labeled cholera toxin B (CTxB), which label PIP_2 and GM1 clusters respectively[13]. By labeling both lipid and protein we are able to monitor movement between nanoscopic lipid domains[16]. To access the PIP_2 on the inner leaflet, the cells were permeabilized (see methods). Cellular staining was verified by confocal microscopy (see Fig. S2a).

Prior to shear, TREK-1_eGFP and GM1 lipids showed strong pair correlation (Fig. 2b,c) suggesting, TREK-1 is associated with or near GM1 lipids. After shear, the pair correlation was dramatically decreased (p<0.01 at 50 nm). A similar experiment with a cy3b labeled anti-TREK-1

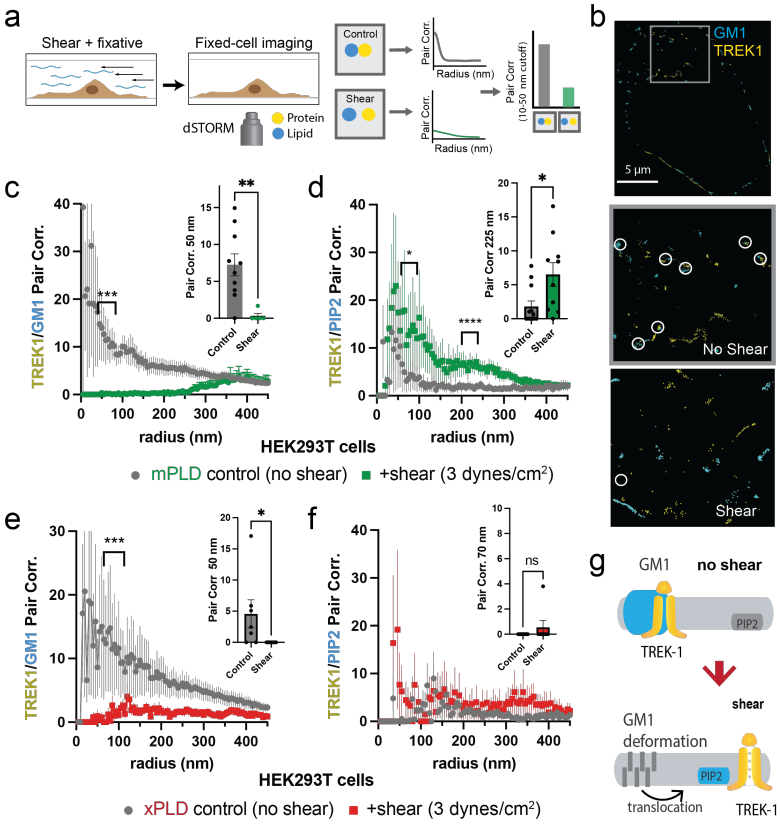

Figure 2 **Shear moves TREK-1 nanoscopic distances in HEK293 cells.** (**a**) A shear fixing protocol is shown. Cell growing in a shear chamber are fixed while shear is applied. Fixed samples are then labeled with fluorescent antibodies or CTxB and imaged for nanoscopic movement (<250 nm) by two-color super resolution imaging and pair correlation (Pair corr.). (**b**) Combined PALM-dSTORM imaging of TREK1_eGFP and Alexa 647 cholera toxin B (CTxB) with and without shear in HEK293T cells. The middle panel, outlined in grey, is the zoomed portion of the cell surface outlined in the top panel. The bottom panel is a zoom of the cell surface from a separate cell treated with shear. Locations of TREK-1/GM1 proximity are outlined with a white circle. (**c**) Pair correlation of TREK1 with GM1 before and after shear (3 dynes/cm^2; green) determined by combined eGFP-dSTORM imaging when mouse phospholipase D2 (mPLD2) is over expressed (non-permeabilized). The significance in the Pair corr. change is shown across the range of radii 50-70 nm (along the curve) and at a single 50 nm radius (inset). (d) combined eGFP-dSTORM imaging of TREK-1_eGFP with Alexa 647 labeled PIP_2 in the presence of over expressed mPLD2 (permeabilized). Significance is shown for radii 70-85 nm along the curve and at a single 225 nm radius (inset). (**e-f**) Combined PALM-dSTORM of TREK-1 in the presence of catalytically dead PLD2 (xPLD2). Shear (3 dynes/cm^2) of TREK-1 is shown as a red curve with xPLD2 present. The experiments are as described in panels c-d. In (e) a significant shift in TREK-1/GM1 pair correlation is shown for 50-70 nm (along the curve) and at a 50 nm radius (inset). In (f) pair correlation did not appear to shift significantly. Significance was determined by a student's t test or for multiple point a nested student's t test; *p<0.05, ** p<0.01, *** p<0.001, ****p<0.0001. (**g**) Cartoon showing TREK-1 movement from GM1 lipids (top) toward PIP_2 lipids (bottom) in response to mechanical shear (red arrow).

antibody showed an almost identical decrease in TREK-1/GM1 pair correlation (Fig. S4a) validating both our eGFP-dSTORM method and the specificity of the TREK-1 antibody (Fig. S2a).

After leaving GM1 lipids, we expect TREK-1 to move a nanoscopic distance to PIP_2 clusters. PIP_2 forms its own nanodomains separate from GM1cluster [13,25,26] which on average are ~133 nm apart in HEK293T cells[27]. Cells were sheared with 3 dynes/cm^2 fluid shear, permeabilized, fixed, and labeled with A647 anti-PIP_2 antibody.

As expected, TREK-1_eGFP pair correlation was low prior to shear and then increased significantly after shear (Fig. 2d), opposite the result with GM1(Fig. 2c). Hence shear causes TREK-1 to leave GM1 cluster and move to PIP_2 cluster. Based on a student's t test, the nanoscopic movement to PIP_2 clusters was significant both at a single radius and a multiple point comparison along the curve. The significance of multiple points was calculated using a nested student's t test (see methods).

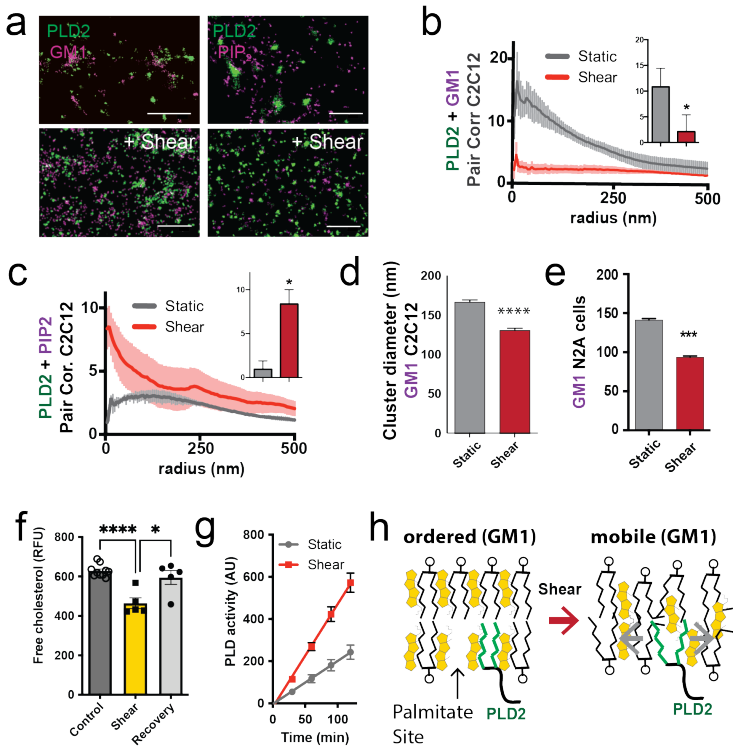

Figure 3. **Shear mobilizes PLD2 within ordered GM1 lipids.** (**a**) two-color dSTORM images of fixed C2C12 cells with and without (3 dynes/cm^2) shear. Cells were labeled with fluorescent CTxB (ganglioside GM1) or antibodies (anti-PIP_2 or PLD2 as indicated) and sheared with the temperature held constant at 37 ℃. Scale bar = 1 µm. (**b**) Cross pair correlation (unitless) of PLD2 with GM1 or PIP_2 lipids at a given radius. Error bars are shown at each point radii. A bar graph (inset) is shown at the shortest calculated radii of 5nm. Prior to shear (grey line) PLD2 is clustered with GM1; after shear there is almost no clustering. (**c**) The opposite was true for phosphatidylinositol 4,5 bisphosphate (PIP_2). Prior to shear, PLD2 is not associated significantly with PIP_2 clusters, after shear PLD2 clustering dramatically increases. (**d**) Cluster analysis of the GM1 (d) and PIP_2 (e) lipids shown in (a). Shear failed to eliminate GM1 or PIP_2 domains after 3 dynes/cm^2 shear force. However, their diameter decreases suggesting force deforms but does not eliminate lipid clusters. (**e**) Cluster analysis of GM1 domains in neuroblastoma 2a (N2a). (**f**) Fluorescent cholesterol assay. N2a cells grown in a 48 well plates were sheared with 3 dynes/cm^2 orbital fluid shear, fixed with shear (10 min), and compared to control cells with no shear using a fluorescent cholesterol assay. After shear, a second set of control cells were allowed to recover with no shear and fixative for 30s (recovery), otherwise the cells were treated identical to experimental cells. (**g**) A live PLD activity assay shows fluid shear (3 dynes/cm^2) increases substrate hydrolysis in cultured N2a cells. (** is $p<0.01$, **** is $p<0.001$, **** is $p<0.0001$, $n>800$ clusters from 5-6 cells). (**h**) Depiction of shear thinning activating PLD2. (left) The palmitates of PLD2 (green lines) are shown bound to the palmitate site in ordered GM1 lipids. (right) After shear cholesterol is reduced and the GM1 lipids are deformed. The deformed surface no longer binds palmitates with the same high affinity, and the palmitates is free to move—a process known as shear thinning.

Next, we investigated shear induced movement of TREK-1 in the presence of xPLD2. Like mPLD2, we over expressed xPLD2 in HEK293T cells matching the conditions of our electrophysiology experiments in Fig. 1b. And like mPLD2, HEK293T cells were sheared, permeabilized, and labeled for two-color dSTORM with eGFP_TREK-1 and either A647-cholesteratoxin or A647-anti-PIP_2 antibody.

In the presence of xPLD2, shear caused TREK-1 to leave GM1 domains (Fig. 2e). However, unlike mPLD2, the association of TREK-1 with PIP_2 clusters remained relatively weak after shear (Fig. 2f) despite an overall increase in TREK-1 and PIP_2 levels in the membrane (Fig. S2c-d). Figure 2g shows a model of shear induced movement of TREK-1 from GM1 PIP_2 clusters.

Mechanism of PLD2 activation by shear.

Presumably TREK-1 moves between nanodomains as a complex with PLD2[12]. TREK-1 is not palmitoylated, rather its binds to PLD2 through its disordered C-terminus. We previously showed PLD2 moves in response to changes in cellular cholesterol, but we have not directly imaged PLD2 movement in the membrane under shear.

To test shear induced movement of PLD2 we used calibrated shear chambers (ibidi μ-Slide $I^{0.4}$ parallel-plate) with cultured C2C12 muscle cells (mouse myocytes) and N2a mouse neuroblastoma cells endogenously expressing TREK-1 (Fig. S2e). The endogenous expression avoids artifacts from saturating GM1 clusters by over expressing the protein. We initiated shear by pumping phosphate buffered saline (PBS) with a calibrated shear of 3 dynes/cm^2. Using a digitally controlled inline heater, the cells were kept at constant 37 ℃. Immediately after applying shear (<10 sec), we infused fixative agents to the shear buffer which allowed the cells to be rapidly fixed in the mechanically stimulated state. Non-sheared control cells were grown and treated similarly on static coverslips without shear (Fig. 3a, S5a).

Using two-color dSTORM and pair correlation, we found shear mobilized PLD2 in the membrane independent of heat. Prior to shear, PLD2 was robustly localized with GM1 clusters (Fig. 3b). After shear, PLD2 pair correlation decreased in GM1 clusters and robustly increased with PIP_2 clusters (Fig. 3c). Shear-induced release of PLD2 from GM1 domains was more robust than anesthetic disruption[14]. The fact that temperature was kept constant, ± 0.1℃, suggests the mechanism is not due to melting of ordered lipids near a transition state.

Cluster analysis of the sheared GM1 particles showed a decrease in the apparent size of GM1 clusters from 167±3 to 131±3 nm (~20%, Fig. 3d) in C2C12 cells and similar effect on the size of GM1 clusters in N2a cells (Fig. 3e). Like GM1 clusters, PIP_2 clusters remained largely intact and slightly smaller (154±1 vs 139±1) after shear (Fig. S5b). The size and number were determined using DBSCAN cluster analysis software of GM1 clusters.

The decrease resembled previous experiments where we removed cholesterol with methybetacyclodextrin[13,14]. To test if mechanical shear lowers cholesterol, we applied orbital fluid shear (3 dynes/cm^2) for 10 min at 37 C and then fixed the cells. Control cells were either not sheard or sheared and then allowed to recover ~45 sec prior to fixing.

We found orbital shear decreased free cholesterol by 25% in N2a cells ($p<0.001$) (Fig. 3f) and this activated PLD (Fig. 3g). The decrease in cholesterol was statistically significant $p<0.0001$ and reversible. Allowing the cells to sit for ~45 prior to fixing increased cholesterol to the levels in non-sheared cells (Fig. 3f). The increase was also significant $p=0.017$.

In C2C12 cells, TREK-1 and PLD2 were well correlated prior to (Fig. S5c, grey trace) and after shear (Fig. S5c, red trace) suggesting they are in a complex at least some of the time in both shear and unsheared states. After shear a small amount of TREK-1 trafficked to PIP_2 (Fig. S5d). Unlike HEK293T cells, C2C12 cells had very little TREK-1/GM1 pair correlation before (Fig. S5e, grey trace). PLD2 is regulated by cholesterol[13] leading us to consider cholesterols role in attracting endogenous levels of TREK-1 to GM1 lipids. In other cell types, we have seen cultured cells have lower cholesterol than human tissues[27,28].

Cholesterol regulation of TREK-1 clustering with GM1 lipids.

Cholesterol, in particular in the brain, can be very high[29]. But nerve cells do not make cholesterol, rather it is made in astrocytes and loaded into nerve cells with apolipoprotein E (apoE), a cholesterol transport protein[28,30]. We reasoned cholesterol could influence endogenous TREK-1 to associate with PLD2 in GM1 clusters. To test this hypothesis, we loaded C2C12 cells with cholesterol using apoE lipidated with 10% serum[27,28,30,31](Fig. 4a). We found lipidated apoE caused TREK-1 to robustly clusters with GM1 lipids in membranes of C2C12 cells (Fig. 4b). This was also true of TREK-1 in N2a cells, and 3 dynes/cm^2 fluid shear completely reversed the effect of cholesterol (Fig. 4d).

Cholesterol induced movement of TREK-1 to GM1 lipids should decrease TREK-1 currents since PLD2 will be inhibited by a lack of substrate. To directly test activity of TREK-1 in high cholesterol loaded conditions, we over expressed TREK-1 in HEK293T cells and measured current density in whole cell patch clamp mode with and without cholesterol uptake (Fig. 4c). Consistent with our model, TREK-1 currents density decreased by almost 2.5-fold in cholesterol loaded cells—the decrease in current was statistically significant ($p< 0.05$).

In earlier studies, we showed astrocytes regulates clustering of proteins in neurons by releasing apoE containing particles loaded

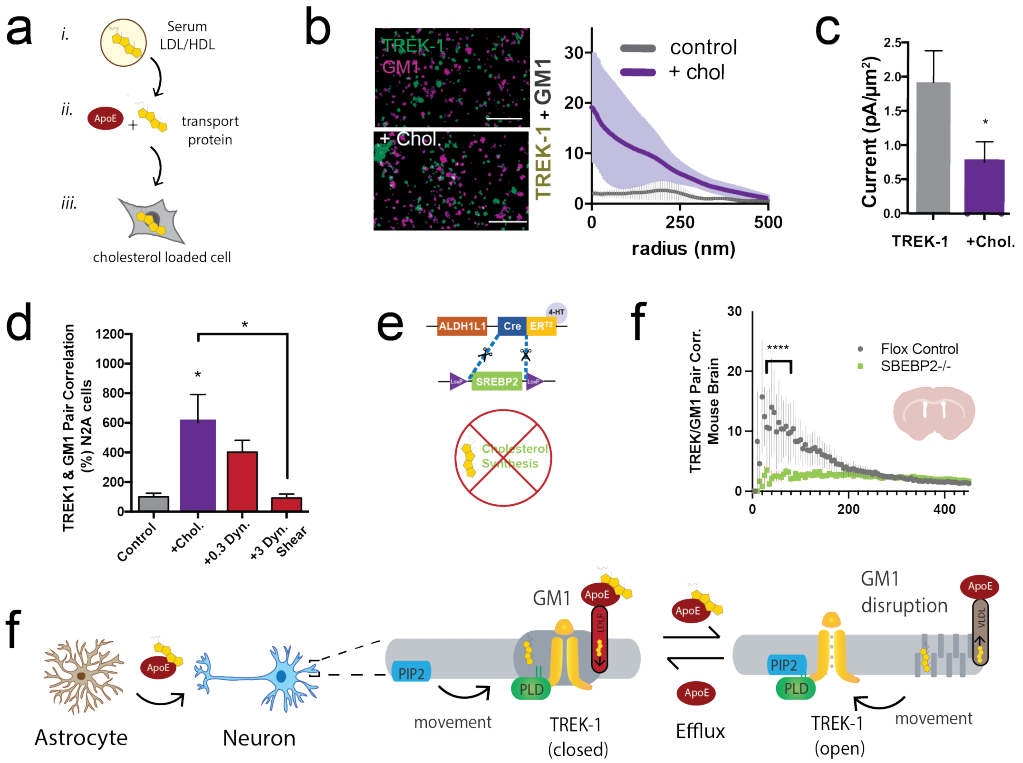

Figure 4. **Astrocyte cholesterol regulates TREK-1 through GM1 clustering.** (**a**) Uptake of cholesterol into cultured cells using the cholesterol transport protein apolipoprotein E (apoE) Panel (**b**) shows cholesterol/lipid uptake into C2C12 cells with 4 µg/ml (~110 nM apoE, purple line. Cholesterol dramatically increases TREK-1 pair correlation of TREK-1 with GM1 labeled lipids. Without cholesterol (grey line) very little TREK-1 was clustered with GM1 lipids. Scale bars = 1 µm. (**d**) Current densities from whole cell patch clamp recordings are shown with and without cholesterol loading with 4 µg/ml apoE in HEK293 cells over expressing human TREK-1. Increasing cholesterol inhibited the channel ~3 fold (unpaired student's t test; *p<0.05) (**e**) Proposed model for cluster associated TREK-1 activation and inhibition. In high cholesterol, TREK-1 clusters with PLD2 and ordered (thick) GM1 lipids inhibiting the channel. In low cholesterol, TREK-1 is partially clustered with PIP_2 generating basal TREK-1 activity (see also Fig. 1C). After shear GM1 clusters (dark grey) are deformed further increasing PLD2 and TREK-1 clustering with PIP_2 lipids (blue).

primarily with cholesterol[30]. In a disease state, cholesterol increased the clustering of proteins at GM1 domains. knocking out cholesterol synthesis in the astrocytes reversed the protein clustering. Presumably, the same astrocyte cholesterol should regulate the TREK-1 localization with GM1 lipids in a mouse brain.

To test for *in vivo* regulation of TREK-1 clustering, we stained 50-micron brain slices from control and astrocyte specific SREBP2 null mice (Fig. 4e). The brains were fixed by whole body perfusion prior slicing. The free-floating brain slices were mounted to circular cover slip with a fiberglass filter paper, which gave dSTORM buffers access to the tissue with almost no background (Fig. S4e). Coronal slices near the hippocampus were stained with cy3b-anti-TREK-1 antibody and A647 CTxB, imaged at unspecified locations (~ 10 regions), and analyzed for pair correlation.

In flox control mice (WT SREBP2), TREK-1/GM1 pair correlation showed TREK-1 clustered near GM1 consistent with the GM1 pair correlation seen in N2a cells (Fig. 4b,f). And as expected, in the astrocyte specific SREBP2 null brains, TREK-1 had very little pair correlation GM1 lipids ($p<0.0001$). These results demonstrate that in the brain of an animal astrocyte cholesterol regulates the affinity of TREK-1 with inhibitory GM1 clusters.

Figure 3f shows a model for TREK-1 regulation by astrocyte cholesterol based on both cultured cells and *ex vivo* experiments. Cholesterol from astrocytes is transported to neurons via apoE[32]. When cholesterol is high, TREK-1 associates with inhibitory GM1 lipids where PLD2 lacks substrate. When cholesterol is low, TREK-1 moves away from GM1 lipids toward activating PIP_2 lipids where PLD2 has better access to its substrate PC and can produce lipid agonists.

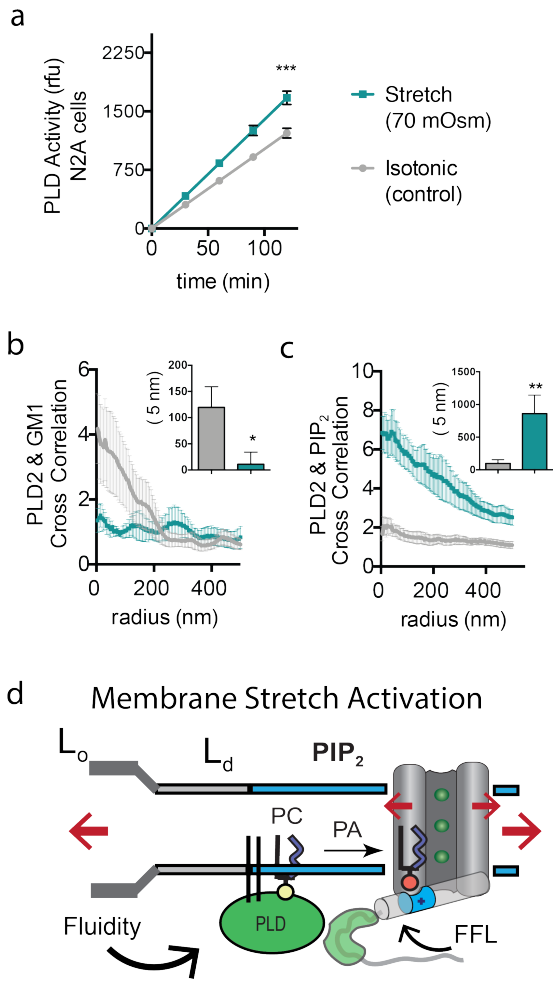

Figure 5. **Osmotic stretch activates PLD2 in N2a cells.** (**a**) Stretch by osmotic swell (70 mOsmo buffer) increased PLD2 catalytic activity in live N2a cells compared to isotonic control cells (310 mOsm) (n=5, p<0.001). (**b-c**) dSTORM imaging showing PLD2 trafficking from ganglioside GM1 to PIP_2 clusters in response to 70 mOsm stretch in N2a cells. Cells were treated, fixed, and labeled with anti-PIP_2 or PLD2 antibody or cholera toxin B (CTxB, GM1). Prior to stretch PLD2 clustered with GM1 lipids and very little with PIP_2 (grey lines). After stretch PLD2 clustered robustly with PIP_2 but very little with GM1 lipids suggesting PLD2 trafficked from liquid ordered domain (Lo), to the liquid disordered domain (Ld). (**d**) Proposed model for TREK-1 stretch activation in a biological membrane by a cluster associated protein activation mechanism (CAPA) and direct force from lipid (FFL). TREK-1 in the open conformation (green ions), in complex with PLD2, is shown after stretch (large red arrows) trafficking (curved black arrow) to PIP_2 clusters (blue shaded bars) in the thin liquid disordered (Ld) region of the membrane (light grey). A known gating helix (grey cylinder) is shown in the up (open channel) position with a PLD2 binding site immediately following the helix (green tube). The opening is a response to three factors that combine to raise the gating helix to the up position. 1) FFL (small red arrows) in TREK-1 favors an open (up) helix conformation. 2) The tip is brought into proximity of PLD2 in the open position and 3) PA (red sphere) is produced and maintains the up positioned by binding to charged residues (blue tube) pulling the helix toward the membrane.

Direct activation of PLD2 by stretch.

In theory fluid shear and stretch should both mechanically perturb the membrane. To confirm stretch activates PLD2, we monitored PLD product release in live cells subjected to hypotonic stretch—cells in low salt buffer swell causing `stretch. We found membrane stretch with 70 mOsm swell increased PLD2 activity ~50% in N2a cells (Fig. 5a). The activation was similar but less dramatic compared to shear in N2a cells (Fig. 3e), which increased ~3-fold in activity.

Next, we tested the ability of stretch to mobilize PLD2 and induce nanoscale movement in the membrane of N2a cells using dSTORM. Cells were treated with either a 70 mOsmo (hypotonic/swell) or 310 mOsmo (isotonic/control) phosphate buffered saline for 15 min at 37 ℃, fixed, labeled, and imaged identically to shear treated cells. Consistent with shear and our PLD2 assay, we saw a clear shift of PLD2 from ordered GM1 clusters to the disordered PIP_2 clusters after osmotic stretch (Fig. 5b-d).

PA regulation of mechanosensitivity thresholds *in vivo*

PLD2 appears to have mechanosensitive properties independent of TREK-1. To establish an independent in *vivo* role for PLD2, we tested mechano-thresholds and pain perception in *D. melanogaster* (fruit flies) devoid of PLD[33]. Flies are a convenient model since they have only one PLD gene and lack a mechanosensitive homolog of TREK-1 (see supplemental discussion). First, we confirmed the neuronally-derived fly cells (BG2-c2) responds to mechanical shear force like cultured mammalian cells. Using our live PLD assay we found 3 dynes/cm^2 shear robustly activates PLD (Fig. 6a). Next, we confirmed that GM1 domains exist in the brain of flies. We found GM1 is expressed throughout the fly brain (Fig. 6b). Whole fly brains were extracted and labeled with CTxB and imaged with confocal.

Next, we tested an *in vivo* role for PA in mechanosensation using single-animal measurements of arousal threshold[34,35] (see Fig.

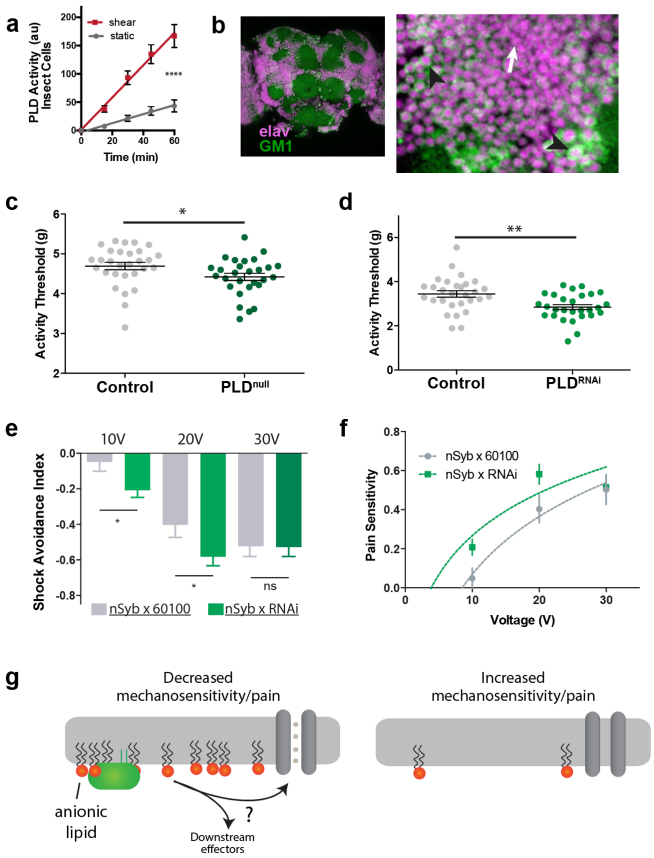

Figure 6. **PA modulates mechanosensitivity in *D. melanogaster*.** (**a**) Shear (3 dynes/cm^2) robustly activates PLD2 in a live PLD assay with cultures neuronal insect cells. (**b**) Cholera toxin robustly labels GM1 lipids (GM1, green), throughout the brain of D. melanogaster. (left). Zoomed section (right) shows that most of the labeling is found on the membrane. There are notable variations in the amount of CTxB labeling with some cells expressing GM1 over the entire membrane (black arrows) while some cells only have labeling in small puncta (white arrow). (**c**) Measurements of *D. melanogaster* mechanosensation in vivo. Animals with or without the pld^{null} gene were stimulated by increasing amounts of mechanical vibration (see supplemental Fig. S4). Flies with lacking PLD2 had a decreased threshold (i.e., more sensitivity to mechanical stimulation) compared to genetically matched controls (w1118) (p=0.039, n= 28-29), consistent with the prediction that PA decreases excitability of nerves. (**d**)The same result was observed in a PLD^{RNAi} line which results in PLD knockdown only in the neurons of *Drosophila* (p=0.002, n=28-29). (**e**) Flies were subjected to increasing voltages of electrical shock in a two-choice assay. PLD-KD flies showed an increased sensitivity to shock when compared with wild-type flies. PLD^{RNAi} flies had a higher aversion to shock at 10V (p=0.0213, n=21) and 20V (p=0.0492, n=27-30), but not at 30V (p=0.672, N=12) (**f**) (**g**) Proposed role of PLD2 in regulating mechanical thresholds. PA is a signaling lipid in the membrane that activates hyperpolarizing channels and transporters. When PA is low the membrane is less polarized, and cells are more sensitive to mechanical activation. The downstream targets are unknown (shown with a '?'). Flies do not have a TREK-1 homolog.

S6a). The arousal-assay measures the amount of mechanical stimulation needed to excite a fly into movement from rest. Flies without functional PLD (PLD^{null}) were subjected to a series of incremental vibrational stimuli every 30 minutes for 24 hours. For each series, the level of stimulation required to arouse the fly, indicated by motion, was recorded using automated machine vision tracking. Averages over the 24 hours were compared to genetically matched controls.

PLD^{null} flies showed a significantly lower arousal threshold than their control strains (Fig. 6c). The lower arousal equates with increased sensitivity to mechanical force. We further used a neuronal-specific driver, Nsyb GAL4, combined with a PLD RNAi line (PLD-KD) to test PLD's role in the central nervous system. Neuronal knockdown of PLD resulted in a similar increase in mechanosensitivity, indicating that the phenotype is neuronal-specific (Fig. 6d).

We also tested the role of PLD in fly shock avoidance as a measure of an adverse electrical stimulus. Responses were measured by placing the PLD-KD flies at the choice-point of a T maze in which they could then choose between a chamber inducing noxious shock or a non-shock control[36]. Flies were subjected to increasing voltages of electrical shock. We found that PLD^{null} flies were more sensitive to electric shock than control (Fig. 6e-f). A potential model for how PA could contribute to mechanosensitivity is shown in Fig. 6g.

Discussion

Taken together we have shown the translocation of TREK-1 and PLD2 nanoscopic distances away from GM1 lipids, and the production of PA near TREK-1, are necessary events associated with full mechanical activation of the channel in cultured cells. In cultured cells, 0.05 PA/cm^2 current density (<10% of the total stretch current) was PLD2 independent (Fig. 1c inset). Presumably, the PLD independent current is from direct mechanical activation of TREK-1, a

mechanism that was first proposed in purified vesicle[22,23]. Some of the PLD2 dependent stretch current may be an enhancement of direct TREK-1 mechanosensitivity; however, the enhancement mechanism is not required as the channel is directly activated by PA in purified lipids absent stretch and tension[37].

The mechanism for TREK-1 nanoscopic movement is both cholesterol dependent (Fig. 4b) and mechanically dependent (Fig. 2), suggesting a shear thinning mechanism of GM1 clusters. Shear thinning is a process where viscous mixtures become more fluid in response to shear or stretch. The process is kinetic and works by mechanical disruption of noncovalent bonds allowing the molecules to move relative to each other (See Fig. 3h, S5f).

Figure S2h shows a proposed model of PLD2 activation by shear thinning. Prior to shear, the ordered GM1 clusters present a surface that is amenable to palmitate binding. This attracts PLD2 to GM1 lipids through an ordered lipid-lipid interaction. When shear is applied, the ordered GM1 lipids deform (shown as bent lipid acyl chains), but they remain ordered. The deformation is shown altering the binding surface for palmitate, which decreases the lipid-lipid interaction and increases PLD2 fluidity in the membrane (see also Supplemental Fig. S3d). The decrease in membrane cholesterol (Fig. 3f) likely evolved to further decrease the palmate order in the palmitate binding site.

The translocation of TREK-1 to PIP_2 clusters appears to be conformation dependent, as the xPLD/TREK-1 combination associated less with PIP_2 after shear compared to the mPLD/TREK-1 combination (Fig. 2d,f) despite an increase in PIP_2 and TREK-1 expression (Fig. S2c-d). This is consistent with the up down model of the gating helix[38]. Figure 5d shows a theoretical mechanism for combined PA signaling and direct force from lipid in a biological membrane. Induced conformational changes are maintained in the helix-up (open) position, only when PLD2 is present and able to produce local PA. If PA is absent, PIP_2 is in higher concentration, which forces the channel closed[37,39] and the helix in the down position (Fig. S3e-f).

The latency of PLD2 dependent activation is important since it indicates the potential physiological processes where PLD2 may function in mechanotransduction. Based on diffusion from GM1 to PIP_2, we estimated a latency of 650 us[13]. In our electrophysiology experiments we cannot rule out an initial fast component from direct TREK-1 mechanosensation (Fig. 1c, inset). Nonetheless, using the rise in TREK-1 activity with wild type PLD2, we calculated a putative upper limit on the time for PLD2 to be activated and generate PA near TREK-1.

After instrument delay we observed initial TREK-1 currents almost immediately and the current appeared significance within 2.1 ms at 60 mmHg (Fig. 1d). This is likely faster than the error in our instrument setup. We did not calibrate the exact error of our setup, but based on estimates from the manufacturer, 10 ms is a very conservative upper limit.

The requirement for both PLD2 activity and the C-terminus to activate TREK-1 by pressure further validates the previous conclusion that TREK-1 is lipid-gated by a local high concentration of PA[12,37]. In theory, PLD2 activity could raise the global PA levels sufficient to activate TREK-1 without being localized through a protein-protein interaction, but we did not see this with truncated TREK-1 and 60 mmHg pressure in HEK293 cells (Fig. 1c).

Many important signaling molecules are palmitoylated including tyrosine kinases, GTPases, CD4/8, and almost all G-protein alpha subunits[40] and palmitoylation alone is sufficient to target proteins to GM1 domains[41]. Translocation of these proteins, or a palmitoylated binding partner, from lipid domains by mechanical force could alter their available substrates and affect downstream signaling. Lipid cluster disruption and its effect on palmitoylated G-proteins likely explains at least some of the mechanosensitivity of many GPCRs[4,7–9] and suggests TREK-1 may share a distant mechanism of activation with many TRP channels[4–6,42]. A common pathway is further suggested by the fact that lipid clustering modulates TRP channels[43,44] and functions downstream of anionic lipid signaling[5]. Many ion channels are also palmitoylated[45]. For example, the voltage-gated sodium channel (Na_v)1.9 clusters with GM1 lipids and its de-clustering (by chemically removing cholesterol) induces a corresponding pain response[46].

PA's regulation of *D. melanogaster* mechanosensation and pain (Fig. 6) adds *in vivo* support to a growing list of anionic lipids that set force-sensing thresholds. For example, PIP_2 sets

the threshold for mechanical B-cell activation[47]. Likewise, sphingosine-1-phosphate (S1P), an anionic lipid similar to PA, regulates pain in mice[48]. PLD's activation by mechanical force and substrate presentation helps explain how anionic lipids could directly set pain thresholds and mechanosensitivity via canonical mechanosensitive ion channels.

Ork1 is the closest homolog to TREK-1 in flies. However, Ork1 is predicted to be most like K2P channels TALK-1 and TALK-2 in humans not TREK-1. In cultured mammalian cells, TALK-1 is insensitive to mechanical stimuli[22] and they are not among the channels that bind PLD2[12]. This suggests that PLD has evolved to regulate distinct mechano-effectors in flies and mammals. A single lipid regulating multiple channels simultaneously may have a greater affect compared to a single channel.

Acknowledgements

We thank Tamara Boto and Seth Tomchik for their assistance in the Drosophila shock experiments, Michael Frohman from Stony Brook for the mouse PLD and mutant PLD cDNA, Steven Long from Memorial Sloan Kettering for human TREK-1-GFP, Padinjat Raghu for the PLD mutant Drosophila, Andrew S. Hansen for PLD experiments, multiple aspects of experimental design and discussion, Yul Young Park for the electrophysiology experimentation, and Carl Ebeling for his help and discussion on the imaging analysis. This work was supported by a Director's New Innovator Award to S.B.H. (DP2NS087943) and R01 (R01NS112534) from the National Institutes of Health, an R01 to W.W.J. (R01AG045036) from the National Institute on Aging, and a graduate fellowship from the Joseph B. Scheller & Rita P. Scheller Charitable Foundation to E.N.P. We are grateful to the JPB Foundation for the purchase of a super resolution microscope. The authors declare no conflict of interest.

Author Contributions

Conceptualization, E.N.P. and S.B.H.; Methodology, E.N.P., M.G., K.R.M, and S.B.H; Investigation, E.N.P., M.G., and K.R.M; Resources, W.W.J., E.M.J., and S.B.H.; Writing – Original Draft, E.N.P. and S.B.H.; Writing – Review and Editing, E.N.P., M.G., M.A.P, E.M.J., and S.B.H.; Supervision, W.W.J. and S.B.H.; Funding Acquisition, W.W.J. and S.B.H.

Works Cited

1. Ranade, S. S., Syeda, R. & Patapoutian, A. Mechanically Activated Ion Channels. *Neuron* **87**, 1162–79 (2015).

2. Julius, D. Molecular mechanisms of nociception . *Nature* **413**, 203–210 (2001).

3. Hahn, C. & Schwartz, M. A. Mechanotransduction in vascular physiology and atherogenesis. *Nat Rev Mol Cell Biol* **10**, 53–62 (2009).

4. Storch, U., Mederos y Schnitzler, M. & Gudermann, T. G protein-mediated stretch reception. *Am. J. Physiol. - Hear. Circ. Physiol.* **302**, H1241-9 (2012).

5. Liu, C. & Montell, C. Forcing open TRP channels: Mechanical gating as a unifying activation mechanism. *Biochem. Biophys. Res. Commun.* **460**, 22–25 (2015).

6. Christensen, A. P. & Corey, D. P. TRP channels in mechanosensation: direct or indirect activation? *Nat. Rev. Neurosci.* **8**, 510–21 (2007).

7. Gudi, S., Nolan, J. P. & Frangos, J. A. Modulation of GTPase activity of G proteins by fluid shear stress and phospholipid composition. *Proc. Natl. Acad. Sci. U. S. A.* **95**, 2515–2519 (1998).

8. Xu, J. *et al.* GPR68 Senses Flow and Is Essential for Vascular Physiology. *Cell* **173**, 762-775.e16 (2018).

9. Wei, W. C. *et al.* Coincidence Detection of Membrane Stretch and Extracellular pH by the Proton-Sensing Receptor OGR1 (GPR68). *Curr. Biol.* **28**, 3815-3823.e4 (2018).

10. Hardie, R. C. & Franze, K. Photomechanical responses in Drosophila photoreceptors. *Science* **338**, 260–3 (2012).

11. Honoré, E. The neuronal background K2P channels: focus on TREK1. *Nat. Rev. Neurosci.* **8**, 251–261 (2007).

12. Comoglio, Y. *et al.* Phospholipase D2 specifically regulates TREK potassium channels via direct interaction and local production of phosphatidic acid. *Proc. Natl. Acad. Sci. U. S. A.* **111**, 13547–52 (2014).

13. Petersen, E. N., Chung, H.-W., Nayebosadri, A. & Hansen, S. B. Kinetic disruption of lipid rafts is a mechanosensor for phospholipase D. *Nat. Commun.* **7**, 13873 (2016).

14. Pavel, M. A., Petersen, E. N., Wang, H., Lerner, R. A. & Hansen, S. B. Studies on the mechanism of general anesthesia. *Proc. Natl. Acad. Sci. U. S. A.* **117**, 13757–13766 (2020).

15. McDermott, M., Wakelam, M. J. O. & Morris, A. J. Phospholipase D. *Biochem. Cell Biol.* **82**, 225–53 (2004).

16. Yuan, Z. & Hansen, S. B. Cholesterol Regulation of Membrane Proteins Revealed by Two-Color Super-Resolution Imaging. *Membranes (Basel).* **13**, 250 (2023).

17. Petersen, E. N., Pavel, M. A., Wang, H. & Hansen, S. B. Disruption of palmitate-mediated localization; a shared pathway of force and anesthetic activation of TREK-1 channels. *Biochim. Biophys. Acta - Biomembr.* **1862**, 183091 (2020).

18. Chemin, J. *et al.* Regulation of the Mechano-Gated K 2P Channel TREK-1 by Membrane Phospholipids. (2007). doi:10.1016/S1063-5823(06)59007-6

19. Patel, A. J. *et al.* A mammalian two pore domain mechano-gated S-like K+ channel. *EMBO J.* **17**, 4283–90 (1998).

20. Brohawn, S. G. How ion channels sense mechanical force: insights from mechanosensitive K2P channels TRAAK, TREK1, and TREK2. *Ann. N. Y. Acad. Sci.* **1352**, 20–32 (2015).

21. Toschi, A. *et al.* Regulation of mTORC1 and mTORC2 complex assembly by phosphatidic acid: competition with rapamycin. *Mol. Cell. Biol.* **29**, 1411–20 (2009).

22. Brohawn, S. G., Su, Z. & Mackinnon, R. Mechanosensitivity is mediated directly by the lipid membrane in TRAAK and TREK1 K+ channels. *Proc. Natl. Acad. Sci. U. S. A.* **111**, 3614–9 (2014).

23. Berrier, C. *et al.* The purified mechanosensitive channel TREK-1 is directly sensitive to membrane tension. *J. Biol. Chem.* **288**, 27307–14 (2013).

24. Schneck, D. J. *Mechanics of Muscle*. *Dynamic Behaviour of Materials Vol 1* (New York University Press, 1992). doi:10.1007/978-3-319-00771-7-1

25. van den Bogaart, G. *et al.* Membrane protein sequestering by ionic protein-lipid interactions. *Nature* **479**, 552–5 (2011).

26. Wang, J. & Richards, D. a. Segregation of PIP2 and PIP3 into distinct nanoscale regions within the plasma membrane. *Biol. Open* **1**, 857–62 (2012).

27. Yuan, Z. *et al.* Hydroxychloroquine blocks SARS-CoV-2 entry into the endocytic pathway in mammalian cell culture. *Commun. Biol.* **5**, 958 (2022).

28. Wang, H. *et al.* The role of high cholesterol in SARS-CoV-2 infectivity. *J. Biol. Chem.* **299**, 104763 (2023).

29. Zhang, J. & Liu, Q. Cholesterol metabolism and homeostasis in the brain. *Protein Cell* **6**, 254–264 (2015).

30. Wang, H. *et al.* Regulation of beta-amyloid production in neurons by astrocyte-derived cholesterol. *Proc. Natl. Acad. Sci. U. S. A.* **118**, e2102191118 (2021).

31. Wang, H., Yuan, Z., Pavel, M. A. & Hansen, S. The role of high cholesterol in aged related COVID19 lethality. *bioRxiv* 2020.05.09.086249 (2020). doi:10.1101/2020.05.09.086249

32. Hansen, S. B. & Wang, H. The shared role of cholesterol in neuronal and peripheral inflammation. *Pharmacol. Ther.* **In press**, 108486 (2023).

33. Thakur, R. *et al.* Phospholipase D activity couples plasma membrane endocytosis with retromer dependent recycling. *Elife* **5**, 1–23 (2016).

34. Murphy, K. R., Park, J. H., Huber, R. & Ja, W. W. Simultaneous measurement of sleep and feeding in individual Drosophila. *Nat. Protoc.* **12**, 2355–2366 (2017).

35. Murphy, K. R. *et al.* Postprandial sleep mechanics in Drosophila. *Elife* **5**, 1–19 (2016).

36. Drago, I. & Davis, R. L. Inhibiting the Mitochondrial Calcium Uniporter during Development Impairs Memory in Adult

Drosophila. *Cell Rep.* **16**, 2763–2776 (2016).

37. Cabanos, C., Wang, M., Han, X. & Hansen, S. B. A Soluble Fluorescent Binding Assay Reveals PIP2 Antagonism of TREK-1 Channels. *Cell Rep.* **20**, 1287–1294 (2017).

38. Brohawn, S. G., Campbell, E. B. & MacKinnon, R. Physical mechanism for gating and mechanosensitivity of the human TRAAK K+ channel. *Nature* **516**, 126–130 (2014).

39. Chemin, J. *et al.* Up- and down-regulation of the mechano-gated K2P channel TREK-1 by PIP2 and other membrane phospholipids. *Pflugers Arch. Eur. J. Physiol.* **455**, 97–103 (2007).

40. Aicart-Ramos, C., Valero, R. A. & Rodriguez-Crespo, I. Protein palmitoylation and subcellular trafficking. *Biochim. Biophys. Acta - Biomembr.* **1808**, 2981–2994 (2011).

41. Levental, I., Lingwood, D., Grzybek, M., Coskun, U. & Simons, K. Palmitoylation regulates raft affinity for the majority of integral raft proteins. *Proc. Natl. Acad. Sci.* **107**, 22050–22054 (2010).

42. Li, Y., Baylie, R. L., Tavares, M. J. & Brayden, J. E. TRPM4 channels couple purinergic receptor mechanoactivation and myogenic tone development in cerebral parenchymal arterioles. *J. Cereb. Blood Flow Metab.* **34**, 1706–14 (2014).

43. Taberner, F. J., Fernández-ballester, G., Fernández-carvajal, A. & Ferrer-montiel, A. Biochimica et Biophysica Acta TRP channels interaction with lipids and its implications in disease ☆. *BBA - Biomembr.* **1848**, 1818–1827 (2015).

44. Morenilla-Palao, C., Pertusa, M., Meseguer, V., Cabedo, H. & Viana, F. Lipid raft segregation modulates TRPM8 channel activity. *J. Biol. Chem.* **284**, 9215–9224 (2009).

45. Shipston, M. J. Ion channel regulation by protein palmitoylation. *J. Biol. Chem.* **286**, 8709–8716 (2011).

46. Amsalem, M., Poilbout, C., Ferracci, G., Delmas, P. & Padilla, F. Membrane cholesterol depletion as a trigger of Nav1.9 channel-mediated inflammatory pain. *EMBO J.* **37**, 1–19 (2018).

47. Wan, Z. *et al.* PI(4,5)P2 determines the threshold of mechanical force-induced B cell activation. *J. Cell Biol.* jcb.201711055 (2018). doi:10.1083/jcb.201711055

48. Hill, R. Z. *et al.* The signaling lipid sphingosine 1-phosphate regulates mechanical pain. *Elife* **7**, e33285 (2018).

49. Brohawn, S. G., del Marmol, J., MacKinnon, R. & del Mármol, J. Crystal Structure of the Human K2P TRAAK, a Lipid- and Mechano-Sensitive K+ Ion Channel. *Science (80-.).* **335**, 436–441 (2012).

50. Su, Z., Brown, E. C., Wang, W. & MacKinnon, R. Novel cell-free high-throughput screening method for pharmacological tools targeting K+ channels. *Proc. Natl. Acad. Sci. U. S. A.* **113**, 1602815113- (2016).

51. Sung, T. C. *et al.* Mutagenesis of phospholipase D defines a superfamily including a trans-Golgi viral protein required for poxvirus pathogenicity. *EMBO J.* **16**, 4519–30 (1997).

52. Piechotta, P. L. *et al.* The pore structure and gating mechanism of K2P channels. *EMBO J.* **30**, 3607–3619 (2011).

53. Thomas, P. & Smart, T. G. HEK293 cell line: A vehicle for the expression of recombinant proteins. *J. Pharmacol. Toxicol. Methods* **51**, 187–200 (2005).

54. Lesage, F. & Lazdunski, M. Molecular and functional properties of two-pore-domain potassium channels. *Am. J. Physiol. Renal Physiol.* **279**, F793–F801 (2000).

55. Tanaka, K. A. K. *et al.* Membrane molecules mobile even after chemical fixation. *Nat. Methods* **7**, 865–866 (2010).

56. Veatch, S. L. *et al.* Correlation functions quantify super-resolution images and estimate apparent clustering due to over-counting. *PLoS One* **7**, (2012).

57. Moon, S. *et al.* Spectrally Resolved, Functional Super-Resolution Microscopy Reveals Nanoscale Compositional Heterogeneity in Live-Cell Membranes. *J. Am. Chem. Soc.* **139**, 10944–10947 (2017).

58. Lang, T. *et al.* SNAREs are concentrated in cholesterol-dependent clusters that define docking and fusion sites for exocytosis. *EMBO Journal* **20**, 2202–2213 (2001).

59. Coltharp, C., Yang, X. & Xiao, J. Quantitative analysis of single-molecule superresolution images. *Curr. Opin. Struct. Biol.* **28**, 112–121 (2014).

60. Robinson, C. V., Rohacs, T. & Hansen, S. B. Tools for Understanding Nanoscale Lipid Regulation of Ion Channels. *Trends Biochem. Sci.* **44**, 795–806 (2019).

61. Raghunathan, K. & Kenworthy, A. K. Dynamic pattern generation in cell membranes: Current insights into membrane organization. *Biochim. Biophys. acta. Biomembr.* **1860**, 2018–2031 (2018).

62. Wang, H., Feng, Z., Del Signore, S. J., Rodal, A. A. & Xu, B. Active Probes for Imaging Membrane Dynamics of Live Cells with High Spatial and Temporal Resolution over Extended Time Scales and Areas. *J. Am. Chem. Soc.* **140**, 3505–3509 (2018).

Materials and Methods

Expression and Purification of TREK-1.

Expression and purification of TREK-1 was performed as previously explained[37]. Briefly, Pichia pastoris (SMD1163H) transformed with the TREK-1 gene in pPICZ-B vector was grown in 2.8L baffled flasks. Overnight cultures were grown overnight at 30C, 250rpm to an OD600 of ~16. Cells are then harvested and resuspended in minimal methanol media and incubation temp is reduced to 25C. Induction was maintained by the addition of 0.5% methanol every 12 hours. Expression was continued for ~48-60 hours. Cells were pelleted, frozen in N2l, and stored at -80C.

Cells were milled and powder was added to lysis buffer (50 mM Tris pH 8.0, 150 mM KCl, 60 mM dodecyl-β-D-maltoside (DDM), 0.1 mg/mL DNAse 1, 0.1 µg/ml pepstatin, 1 µg/ml leupeptin, 1 µg/ml aprotinin, 0.1 mg/ml soy trypsin inhibitor, 1 mM benzamidine, and 0.1 mg/ml AEBSF, with 1 mM phenylmethylsulfonyl fluoride added immediately before use) at a ratio of 1g pellet/4mL lysis buffer. After stirring for 4 hours membranes were extracted at 35,000 xg for 45 min and supernatant was applied to cobalt resin (Clontech) column by gravity flow. Column was serially washed and eluted in IMAC buffer (50 mM Tris pH 8.0, 150 mM KCl, 4 mM DDM, pH 8) with 30 mM and 300 mM imidazole respectively. Eluted protein was concentrated and applied to Superdex 200 column (GE Healthcare) equilibrated in buffer (20 mM Tris pH 8.0, 150 mM KCl, 1 mM EDTA, 2 mM DDM).

Flux Assay

The flux assay was performed similarly as previously published[49]. Briefly, 5 µL of sonicated proteoliposomes was added to 195 µL of flux assay buffer (150mM NaCl, 20mM HEPES pH 7.4, 2µM ACMA) in duplicates in a black 96-well plate (Costar 3915). A protocol was set up on a Tecan M200 Pro to initially read the fluorescence (excitation 410, emission 490) every twenty seconds for one minute as a baseline. The temperature inside the plate reader was set at 25°C. Then, using the protonophore CCCP (1µM final concentration), we collapsed the electrical potential allowing protons into the vesicles. Fluorescence was read every twenty seconds for seven minutes. Next, the potassium-selective ionophore valinomycin (20nM final concentration) was added to terminate the chemical gradient, and fluorescence was read every twenty seconds for five to ten minutes. An average of the duplicates was taken, and then the data was normalized similar to that published in Su et al [50]. Briefly, at each time point $(F-F_{start})/(F_{start} - F_{end})$ was calculated, where F is the fluorescent value at that time, F_{start} is the average of the first four initial readings before the addition of CCCP, and F_{end} is the final fluorescent value after 5 minutes of valinomycin. Next, control proteoliposome flux was normalized to 1 throughout CCCP, and the TREK flux was normalized to the control accordingly. In flux assay figures, addition of CCCP occurs at t=80 seconds and ends at t=520 seconds before valinomycin was added.

Cell Culture and Gene Expression

HEK293t cells (ATCC Cat# CRL-3216, RRID:CVCL_0063) were maintained in the solution consisting of the DMEM (Corning cellgro) culture media, 10% FBS, 100 units/mL penicillin, and 100 µg/mL streptomycin. Cells were plated on poly-D-lysine-coated 12 mm microscope cover glass ~12h, ~36h, or ~60 h before transfection in low confluence (5%, 2.5%, or 1.25%). Genes for target proteins were transiently co-transfected to HEK293t cells with X-tremeGENE 9 DNA transfection agent (Roche Diagnostics). Full-length human TREK-1(hTREK-1) with C-terminus GFP tag in pCEH vector was a gift from Dr. Stephen Long. Mouse PLD2 constructs(mPLD2) without GFP tag in pCGN vector were gifts from Dr. Michael Frohman. Both functional (mPLD2) and inactive mutant (mPLD2-K758R, single mutation) form of mPLD2 were used together blindly to test mPLD2 effect on hTREK-1. hTREK-1 was co-transfected with mPLD2 or K758R with the 1(0.5g of hTREK-1):4(2g of PLD2) ratio[12]. All the salts for internal/external solutions were purchased from either Sigma or Fisher Scientific.

Electrophysiology

The transfected HEK293t cells were used in 24~36 hr. after transfection. Standard excised inside-out patch-clamp recording procedure for TREK-1 was performed following the lead of others (Brohawn et al., 2014; Honore et al, 2006; Coste et al., 2010). Currents were recorded at room temperature with Axopatch 200B amplifier and Digidata 1440A (Molecular Devices). Borosilicate glass electrode pipettes (B150-86-10, Sutter Instrument) were pulled with the Flaming/Brown micropipette puller (Model P-1000, Sutter instrument) resulting in 3~6 MΩ resistances with the pipette solution (in mM): 140 NaCl, 5 KCl, 1 CaCl2, 3 MgCl2, 10 TEA-Cl, 10 HEPES, pH 7.4 (adjusted with NaOH). Bath solution consists of (in mM): 140 KCl, 3 MgCl2, 5 EGTA, 10 TEA-Cl, 10 HEPES, pH 7.2 (adjusted with KOH). Low concentration of TEA (10 mM), which has been known to be insensitive to TREK-1 current (Piechotta et al., 2011), was added into both pipette/bath solutions to block the endogenous potassium channels in HEK293 cells (Thomas and Smart, 2005). Patch electrodes were wrapped with parafilm to reduce capacitance. Currents measured using Clampex 10.3(Molecular Devices) were filtered at 1 kHz, sampled at 20 kHz, and stored on a hard disk for later analysis. Pressure clamping on the patch was performed using high speed pressure clamping system (ALA Scientific) through the Clampex control. Data was analyzed off-line by a homemade procedure using IgorPro 6.34A (WaveMetrics).

hTREK-1 current either co-expressed with mPLD2 or K758R was activated by negative pressure steps from 60 to 0 mmHg in 10 mmHg decrements at +30 mV membrane potential, and 5 traces for each case were recorded and averaged for the analysis. Inside-out patch has generally less patch size variability than cell-attached recording when pressure clamped (Suchyna et al., 2009), but in other to further minimize the patch size variability in inside-out patches, patch size was estimated using a method described by Sakman and Neher (Sakman and Neher,1995), and the current density (I_density; pA/µm^2) was calculated for the further analysis. Then, a Boltzman equation, I_density = base +{max/[1+exp((P50-P)/slope)]} was used to fit the data with a constraint of base=1 due to poor saturation of the current at high pressure. P is the applied pressure, P50 is the pressure that activates 50% of maximum current, and slope shows the sensitivity of current activation by pressure. In some experiments with hTREK-1+K758R co-expression where the activated currents were too small to fit to the Boltzman equation, the current amplitude at P=-30 mmHg (I_m30) was compared with its 5x standard deviation(I_5xSD). If I_m30 < I_5xSD, the experiment was excluded from the Boltzman equation fitting and

corresponding P50-slope analysis. This empirical rule (we call it 5xSD rule) can discern 4 out of 5 wilt type cell-attached recording cases as null experiments suggesting that it could be a usable/useful empirical criterion for our experiment. Then, the current density at -60 mmHg and P50-slope data were used for statistical analysis. Mann Whitney test was done to assess statistical significance using Prism6 (GraphPad software), and outliers were eliminated using a built-in function in Prism with Q = 1 %. The values represented are Mean +/- SEM.

TREK-1 Whole Cell Recordings

Cell Culture and Gene Expression. HEK293t cells were maintained in the solution consisting of the DMEM (Corning Cellgro) culture media, 10% FBS, 100 units/mL penicillin, and 100 µg/mL streptomycin. Cells were plated on poly-D-lysine-coated 12 mm microscope cover glass ~12h, ~36h, or ~60 h before transfection in low confluence (5%, 2.5%, or 1.25%). Genes for target proteins were transiently co-transfected in HEK293t cells with X-tremeGENE 9 DNA transfection agent (Roche Diagnostics). Full-length human TREK1 with C-terminus GFP tag in pCEH vector was a gift from Dr. Stephen Long. Mouse PLD2 constructs without GFP tag in pCGN vector were gifts from Dr. Michael Frohman. Both functional PLD2 and inactive mutant PLD2-K758R[51], single mutation form of mPLD2 were used together blindly to test PLD2 effect on TREK1. TREK1 and PLD2 were co-transfected 1(0.5 µg):4(2 µg) ratio[12], otherwise a total 1 µg of DNA was used in transfection.

Electrophysiology. The transfected HEK293t cells were used in 18~24 (TREK1 expression) or 24 ~ 30 (TREK1 + PLD2 co-expression) hours after transfection. Standard whole-cell patch-clamp procedure for TREK1 was performed according to previous studies[12,22]. Currents were recorded at room temperature with Axopatch 200B amplifier and Digidata 1440A (Molecular Devices) on a Windows7 based personal computer. Borosilicate glass electrode pipettes (B150-86-10, Sutter Instrument) were pulled with the Flaming/Brown micropipette puller (Model P-1000, Sutter instrument) resulting in 4~7 MΩ resistances with the internal solution (in mM): 140 KCl, 3 $MgCl_2$, 5 EGTA, 10 HEPES, pH 7.4 (adjusted with KOH). External solution consists of (in mM): 145 NaCl, 4 KCl, 2 $CaCl_2$, 1 $MgCl_2$, 10 HEPES, pH 7.4 (adjusted with NaOH). TEA (10 mM), which has been known to be insensitive to TREK1 current[52], was added into both internal/external solutions to block the endogenous potassium channels in HEK293 cells[53]. Patch electrodes were wrapped with parafilm to reduce capacitance, and series resistance was compensated by ~70% (both prediction and correction). Currents measured using Clampex 10.3 (Molecular Devices) were filtered at 2 kHz, sampled at 10 kHz, and stored on a hard disk for later analysis. Data was analyzed off-line by a homemade procedure using IgorPro 6.34A (WaveMetrics). Currents were elicited by a biphasic step voltage command (at -10 and -100 mV from V_{hold} = -60 mV) and ramp voltage commands (short ramp = -120 mV to -10 mV in 440 ms, and long ramp = -100 mV to +50 mV in 1 sec) in absence and presence of quinidine (200 µM), which was used as a known TREK1 blocker[54]. The subtracted 200 µM quinidine sensitive currents from the long ramp were used to obtain the current density at 0 mV. Mann Whitney test was done to assess statistical significance using Prism6 (GraphPad software), and outliers were eliminated using a built-in function in Prism with Q = 1 %.

Cell Culture

All cells were grown in Dulbecco's Modified Eagle Medium (DMEM) containing 10% fetal bovine serum (FBS) and 1% penicillin/streptomycin unless otherwise noted. C2C12 cells (ATCC Cat# CRL-1772, RRID:CVCL_0188) were changed to a serum-free media containing no FBS or antibiotics 24 hours prior to experimentation unless otherwise noted. For the in vivo assay, PBS-glucose buffer contained D-glucose (20mM) in PBS (VWR, 45000-446).

Fixed cell preparation

C2C12 cells were grown to 80% confluence and then allowed to differentiate overnight in serum free media. Cells were rinsed, treated as needed, and then fixed with 3% paraformaldehyde and 0.1% glutaraldehyde for 10 min to fix both protein and lipids. Glutaraldehyde was reduced with 0.1% NaBH4 for 7 min followed by three-10 min washes with PBS. Cells were permeabilized for 15 min with 0.2% Triton X-100, blocked with 10% BSA/0.05% Triton/PBS at rt. for 90 min. Primary antibody (PLD2, Cell Signaling #13891; TREK-1, Santa Cruz #sc-50412; PIP_2, Echelon Biosciences #z-P045) was added to a solution of 5% BSA/0.05% Triton/PBS for 60 min at rt at a concentration of 1:100 followed by 5 washes with 1%BSA/0.05% Triton/PBS for 15 min each. Secondary antibody (Life Technologies #A21244 and A21235; cy3B antibodies were produced as described previously[13]) was added in the same buffer as primary for 30 min at rt followed by 5 washes as above. A single 5 min wash with PBS was followed by a post-fix with fixing mixture, as above, for 10 min w/o shaking. This was followed by three-5 min. washes with PBS and two-3 min. washes with dH2O. Cells only receiving CTxB treatment were not permeabilized.

The dual-fixation protocol is used to minimize any effects from post-fixation aberrations. While always good practice for super-resolution in general, this dual fixation also ensures that the movement of any molecule of interest which may not have been immobilized by the initial fixation can be fully immobilized after labeling since the antibodies or toxins used for labeling will be efficiently cross-linked during this post-labeling fixation step. While some have proposed that this problem should be solved by adding the label before the initial fixation[55] we believe that in the absence of easily-attainable monomeric labeling molecules it would have likely led to clustering artifacts due to the (often) multimer nature of the labeling proteins.

For cells loaded with cholesterol, 4 ug/mL apolipoprotein E3 (BioLegend, USA) was mixed with fresh 10% FBS and applied to the cells for 1hr prior to shear and or fixing.

Shear force was applied to cells in ibidi µ-Slide $I^{0.4}$ Luer chambers with a flow rate calibrated to apply 3.0 dynes/cm^2. Fixation media (see above) was applied to cells using a syringe pump (Harvard Apparatus PHD ULTRA) and kept at 37°C using an in-line heater (Warner SH-27B).

TREK-1 in HEK293T cells was labeled with a eGFP concatenated to the C-Terminus of full-length human TREK-1 (Fig. S3b), or by applying anti-TREK-1 antibody (sc-398449, Santa Cruz) conjugated to cy3b[13]. Anti-PIP_2 antibody was directly conjugate alexa 647 using the same protocol.

Imaging Protocols

Super-resolution dSTORM imaging

Images were recorded with a Vutara 352 and VXL super-resolution microscopes (Bruker Nano Surfaces, Salt Lake City, UT) which is based on the 3D Biplane approach. Super-resolution images were captured using a Hamamatsu ORCA Flash4.0 sCMOS camera and a 60x water objective with numerical aperture 1.2. Data were analyzed by the Vutara SRX software (version 5.21.13). Single molecules were identified by their brightness frame by frame after removing the background. Identified particles were then localized in three dimensions by fitting the raw data in a customizable region of interest (typically 16 X16 pixels) centered on each particle in each plane with a 3D model function that was obtained from recorded bead data sets. Fit results were stored as data lists for further analysis.

Fixed samples were imaged using a 647 nm and 561 nm excitation lasers, respectively, and 405 nm activation laser in photo switching buffer comprising of 20 mM cysteamine (Sigma, #30070), 1% betamercaptoethanol (BME) (Sigma, #63689) and oxygen scavengers (glucose oxidase, GLOX) (Sigma #G2133) and catalase (Sigma #C40)) in 50mM Tris (Affymetrix, #22638100)+10 mM NaCl (Sigma, #S7653) +10% glucose (Sigma, #G8270) at pH 8.0 at 50 Hz and maximal powers of 647 nm, 561 nm and 405 lasers set to 8, 10, and 0.05 kW cm-2 respectively. Live cell imaging was performed in DMEM supplemented with oxygen scavengers and 0.1% betamercaptoethanol in 50mM Tris+10mM buffer +2% glucose. An autocorrelative algorithm[38] was used to correct for drift correction.

eGFP-STORM. The eGFP and either A647 CTxB or A647 PIP_2 were excited with a 488 and 640 lasers respectively with no 405 activation in GLOX/BME buffer. The GLOX/BME buffer was not required for eGFP blinking, but it did improve the fluorescence and the number of localization particles determined. The resolution of eGFP_TREK-1 and cy3b labeled anti TREK-1 were comparable (47±14 nm vs. 38±6 respectively).

Pair correlation and cluster analysis was performed using the Statistical Analysis package in the Vutara SRX software. Pair correlation analysis is a statistical method used to determine the strength of correlation between two objects by counting the number of points of probe 2 within a certain donut-radius of each point of probe 1. This allows for localization to be determined without overlapping pixels as done in traditional diffraction-limited microscopy. Localization at super resolution is beyond techniques appropriate for diffraction-limited microscopy such as Pearson's correlation coefficient.

The resolution of dSTORM images was calculated with the resolution analysis feature of the VutaraSRX software. The resolution was calculated in the xy plane using 10 nm pixel size for each cell used for pair correlation and the mean determined.

Fluorescence Recovery After Photobleaching (FRAP)

For fixation studies N2a and C2C12 cells were grown in DMEM with 10% FBS until 16 hours before use in which they were switched into serum free DMEM. On the day of the experiment, DMEM in live cells was replaced with DMEM w/o phenol red. Fixed cells were rinsed once with PBS and then put into a mixture of PBS with 3% PFA and 0.1% glutaraldehyde for 20 min at 37C. Fixed cells were then rinsed with PBS 5 x 5 min and then placed back into phenol-free DMEM. CTxB (ThermoFisher C34778, 100 ug/ml) was then applied 1:200 into each plate and allowed to incubate for >30 min before imaging. Imaging and data collection was performed on a Leica SP8 confocal microscope with the Application Suite X v.1.1.0.12420. 5 images were taken as baseline after which a selection of 1 or more ROI was bleached at 100% laser power for 6-8 frames. Recovery was measured out to 5 min and fluorescence of the ROI(s) were quantified. The fluorescence before bleaching was normalized to 1 and after the bleaching step was normalized to 0.

Cholesterol Assay

N2a cells were cultured in 48 well plates with 200uL media in each well and then changed to 200uL PBS for the shear treatment. The shear plate was incubated with PBS on an orbital rotator at 3dyn/cm^2 for 10 min in a 37°C incubator. The control plate was incubated with PBS for 10 min in the same incubator with no shear. Then the shear plate was incubated with 200uL 4%PFA+0.1% glutaraldehyde in PBS for 10 min with 3dyn/cm^2 shear and 10 min without shear. The control plate was fixed for 20 min with no shear.

In vitro cellular PLD Assay

In vitro cellular PLD2 activity was measured in cultured HEK293T cells by an enzyme-coupled product release assay[13] using amplex red reagent. Cells were seeded into 96-well plates (~5×10^4 cells per well) and incubated at 37 °C overnight to reach confluency. The cells were starved with serum-free DMEM for a day and washed once with PBS (phosphate-buffered saline). The PLD reaction was initiated by adding 100 µL of reaction buffer (100 µM amplex red, 2 U/ml horseradish peroxidase (HRP), 0.2 U/ml choline oxidase, and 60 µM C8-PC in PBS). The assay reaction was performed for 2-4 hour at 37 °C and the activity was kinetically measured with a fluorescence microplate reader (Tecan Infinite 200 Pro) at excitation and emission wavelengths of 530 nm and 585 nm, respectively. The PLD2 activity was calculated by subtracting the background activity (reaction buffer, but no cells). For the bar graphs, samples were normalized to the control activity at the 120 min time point.

Drosophila Assays

For behavior experiments, 1 to 5-day old flies were collected in vials containing ~50 flies at least 12 hours before the experiment. Flies were allowed to acclimate to behavior room conditions for >30 min (dim red light, ~75% humidity) before each assay. Shock avoidance was tested by placing flies in a T-maze where they could choose between an arm shocking at the indicated voltage every 2 seconds and an arm without shock. Flies were given 2 min to choose which arm, after which flies were collected and counted to determine the shock avoidance index for each voltage and genotype. Control and knockout flies were alternated to avoid any preference and the arm used for shock was also alternated to control for any non-shock preference in the T-maze itself. Shock avoidance index (AI) was calculated as AI=(# flies shock arm-# flies control arm)/# flies total. Plotting the inverse of this metric we obtain a

pain sensitivity curve in which we observe a right-shift when the *pld* gene was knocked down (Fig. 3f).

Arousal threshold protocol has been described in detail previously[35]. Briefly, animals were exposed hourly to a series of vibrations of increasing intensity ranging from 0.8 to 3.2 g, in steps of 0.6 g. Stimuli trains were composed of 200 ms vibration with 800 ms inter-vibration interval and 15 s inter-stimuli train interval. Stimulation intensity and timing were controlled using pulse-width modulation via an Arduino UNO and shaftless vibrating motors (Precision Microdrives, model 312–110). Arousal to a given stimulus was assigned when an animal (1) was inactive at the time of the stimulus, (2) satisfied a given inactivity criteria at the time of the stimulus, and (3) moved within the inter-stimuli train period (15 s) of that stimulus.

Statistics

All statistical calculations were performed using a student's t-test in Prism software (v9) unless otherwise noted. For statistics of more than one point along a pair correlation curve a nested students t-test was used. Significance is noted as follows: ns: $p>0.05$; *:$p<0.05$; **:$p<0.01$; ***:$p<0.001$; ****$p<0.0001$.

Supplemental Discussion

Cholera toxin labeling: The cholera toxin and antibody probes used to label the lipids in our study have been shown to cause artificial clustering in unfixed cells[17,56,57]. Clustering of proteins in unfixed cells is called “antibody patching”. Antibody patching has been used in the past to segregate proteins into distinct compartment for determining their localization in a biological membrane[16,58]. Here we expect antibody patching to have the same effect on lipids which would provide a beneficial effect for clearly determining localization of proteins with lipids in the membrane.

Nonetheless, to mitigate other potential artifacts from clustering, cells were fixed twice, once during treatment to decrease lipid movement, and then again after labeling to ensure good dSTORM localization precision. We tested diffusion after fixing using our typical experimental setup and procedures. In our system, fixing with combined paraformaldehyde and glutaraldehyde effectively inhibited diffusion of GM1 lipids as measured by fluorescence recovery after photobleaching (FRAP) (Fig. S5g-h)).

Potential artifacts resulting from differences in labeling density and overcounting are also possible artifacts. This could impact the size of the lipid clusters we analyzed in Fig. 3. We quantified the amount of fluorescent labeling in Fig. S3h. A small decrease in labeling was observed after shear, but the change was not statistically significant. The translocation of PLD2 between domains was determined by cross-correlation analysis which is not subject to artifacts from changes in labeling density[59]. Hence, our data showing a movement of proteins between domains is largely independent of artifacts arising from any artificial clustering[17,57,60]. This conclusion is also supported by the similar dSTORM results obtained from eGFP and cy3b-anti-TREK-1 antibody (Fig. 2, S4).

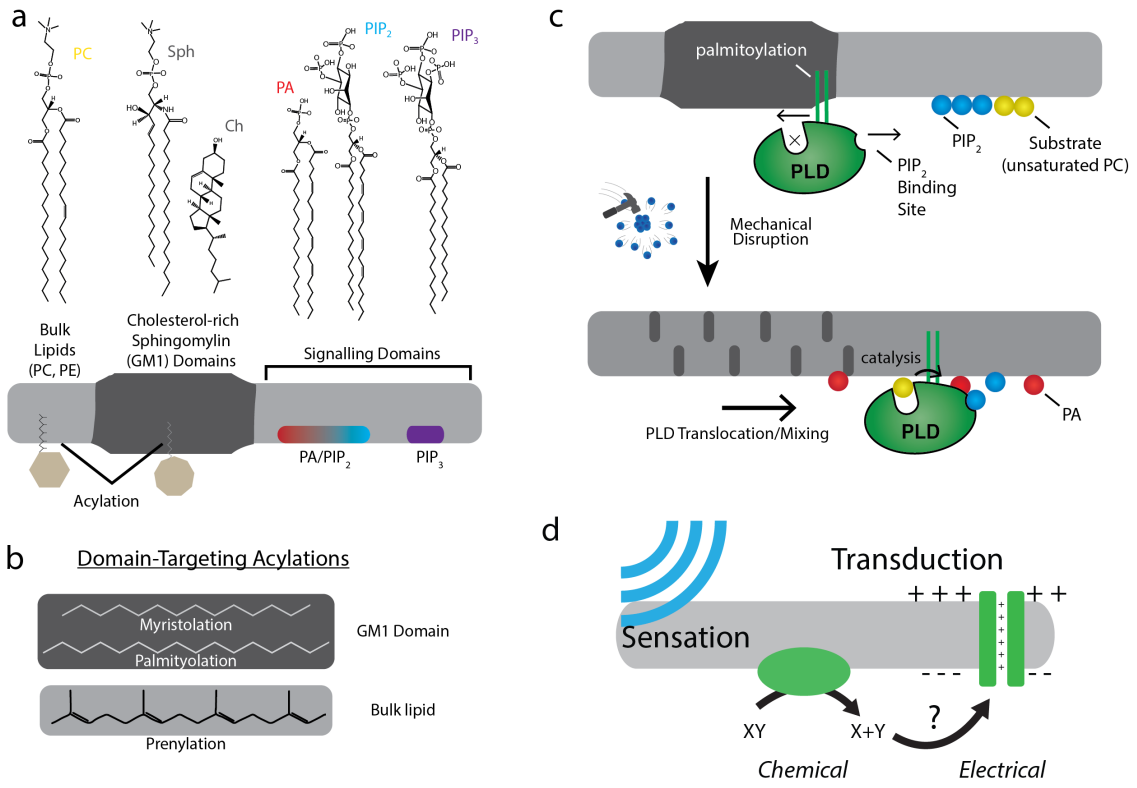

Supplemental Figure 1. **The role of lipids and lipid order in mechano-transduction.** The plasma membrane is composed of lipids which can cluster into separate and distinct domains with unique properties such as thickness and charge (**a**). These domains contain proteins which localize to them through post-translational acylation (**b**). Domain localization exposes proteins to micro-environments which can regulate their activity. For example, our previous findings showed that PLD is localized to GM1-labeled domains due to its palmitoylation sites (**c**, top). This sequesters PLD from high concentrations of substrate (phosphatidylcholine) and activating lipid (PIP_2). Upon chemical or mechanical disruption of the domain, the environment changes, instead favoring PLD translocation and activation (**b**, bottom) by substrate presentation. This process is a form of cellular transduction. (**d**) Transduction is known to occur directly between a mechanical to chemical signal using raft-localized enzymes, but it is unknown whether electrical transduction also occurs directly or can be facilitated through a secondary mechanism.

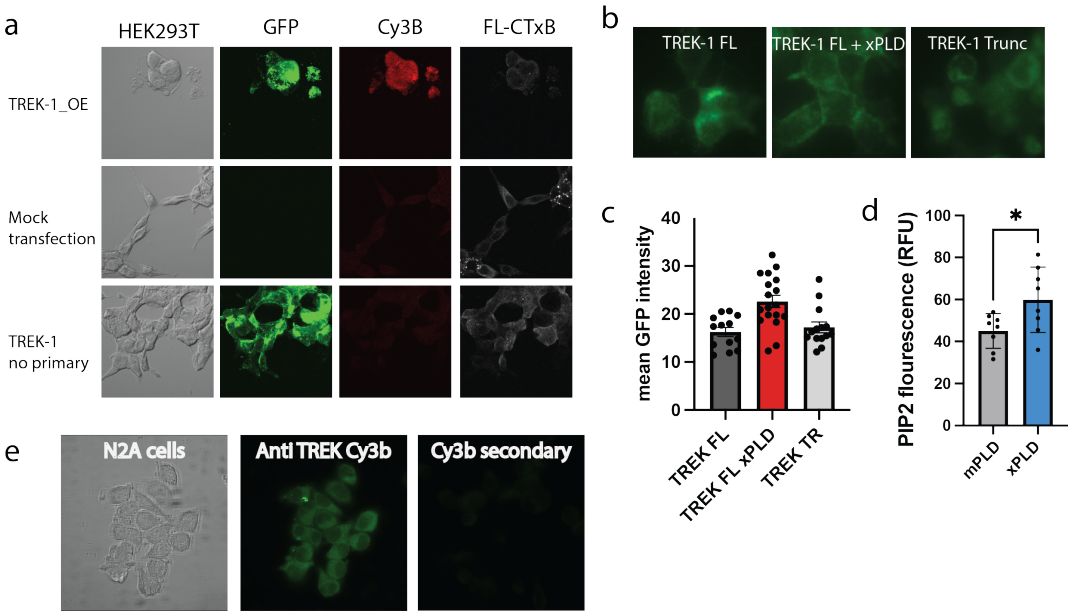

Supplemental Figure 2. **Expression and staining of TREK-1 in cell culture.** (a) Confocal imaging of HEK293T cells over expressing an eGFP tagged human TREK-1. Cells were fixed and stained with anti-trek antibody and a secondary cy3b antibody and A647 conjugated cholesterol toxin B (CTxB). Without transfection no GFP is visible. A negative control (no primary antibody) has no fluorescence. (b) Over expressed eGFP-TREK-1 in HEK293 cells (identical to those used in Fig. 1, can be seen in the plasma membrane of each construct used for electrophysiology. (**c-d**) over expressing catalytically dead PLD2 (xPLD), appears to slightly increase the amount of TREK-1 expression. Truncating the c-terminus (TREK trunc) has no effect on expression at the plasma membrane.

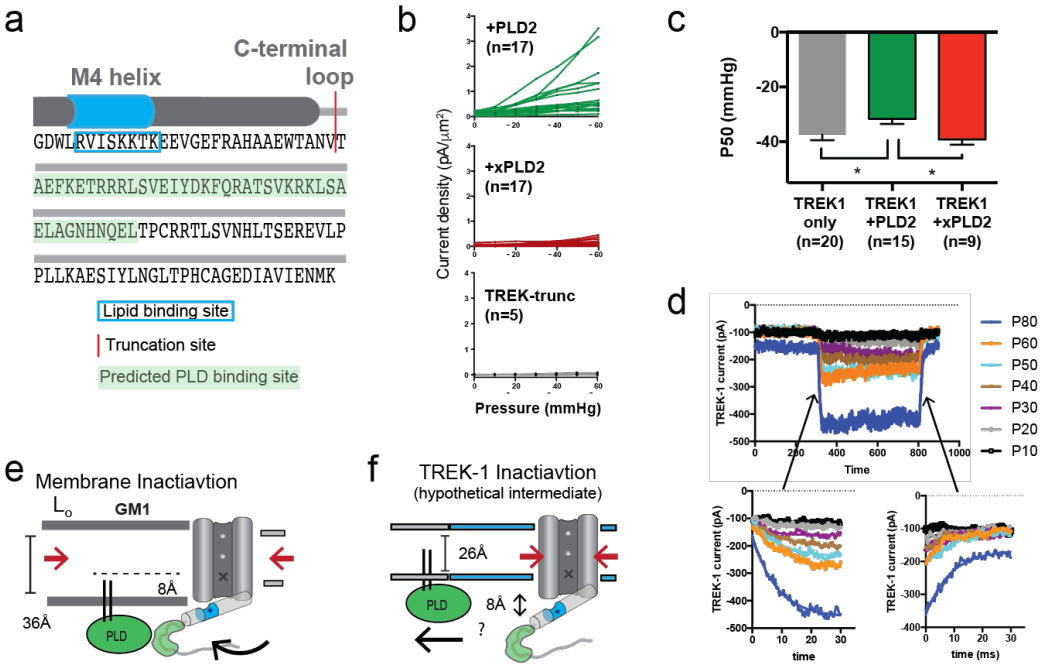

Supplemental Figure 3. **Electrophysiology details and methods.** (**a**) Diagram of the C-terminal end of TREK-1 showing the truncation site (red) used and the predicted PLD binding site for PLD2. The last transmembrane helix (M4) is shown as a grey cylinder, and the anionic lipid binding site is highlighted in blue. (**b**) Individual cell traces for TREK-1+PLD2 (green), TREK-1+xPLD2 (red), and TREK-1-truncated (grey) current densities (pA/μm^2). (**c**) The pressure required to open TREK-1 is decreased when PLD is overexpressed ($p<0.05$, n=15-20). The observation is coming from very little current (red traces in panel a). (**d**) Representative cell showing TREK-1 pressure currents (0-60 in 10 mmHg increments). Bottom left is activation step, bottom right is deactivation. Both activation and inhibition appear to be sub 5 ms processes, which is at the limit of detection for our instrument setup. (**e**) Membrane inactivation. After stretch, the membrane relaxes and palmitates from PLD2 regel with the GM1 lipids and TREK is pulled into GM1 clusters through its interaction with PLD2 (see Fig. 3e for evidence of a complex in GM1 clusters). Absent PA and due to increased hydrophobic thickness of the membrane, the gate is in the down (closed position, marked with an X). (**f**) Direct inactivation of TREK-1 through an intermediate. Release of stretch could in theory force the channel into a closed conformation by a large amount of direct pressure on the channel (large red arrows). In a thin membrane this would cause the helix to move up to 8 Å away from the membrane and potentially disrupt the PLD2/TREK-1 interaction allowing PLD2 to translocate back to GM1 lipids. This would be an intermediate as TREK-1 would likely re-associate in the thick lipids.

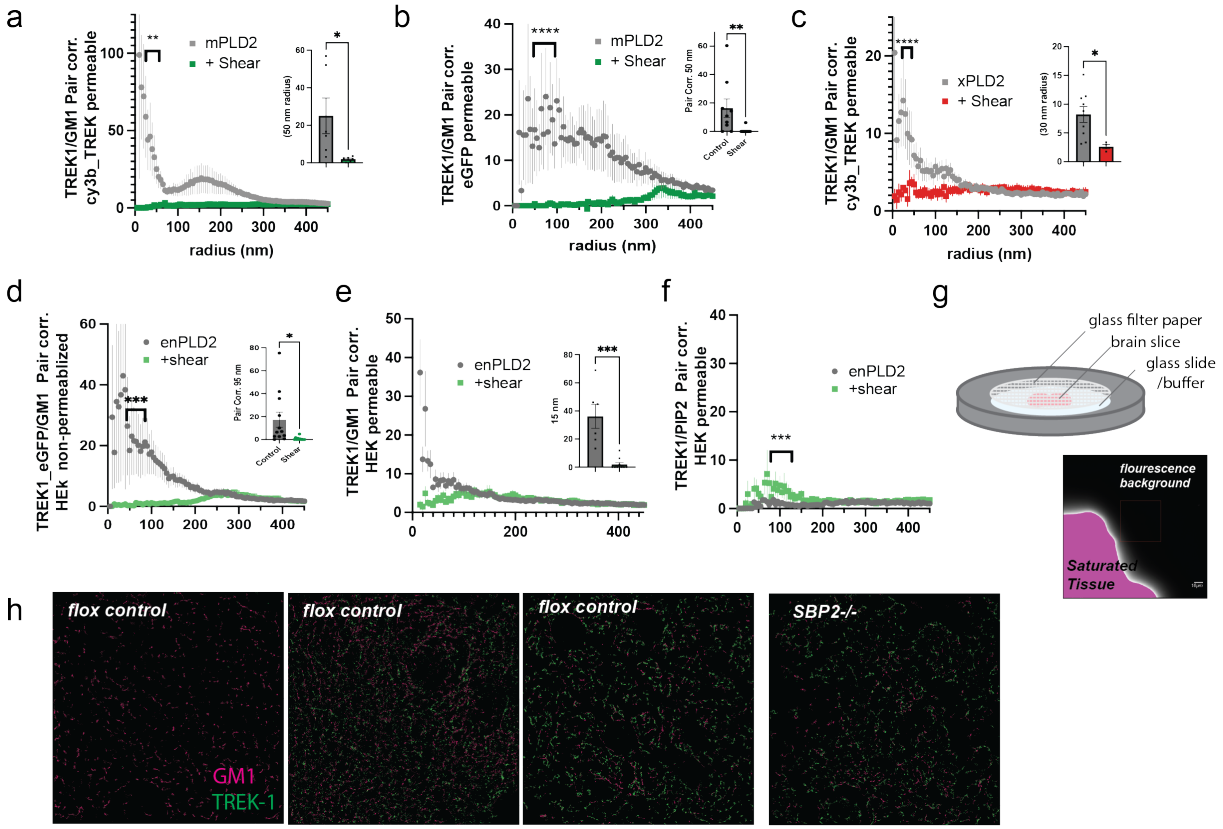

Supplemental Figure 4**. Comparisons of labeling type and permeabilization.** (**a**) dSTORM with cy3b labeled TREK-1 antibody after shear in the presence of over expressed mouse PLD2 (mPLD2) with full length human TREK-1. HEK293T cells were fixed, permeabilized, and stained with a Cy3b conjugated anti-TREK-1 antibody. Pair correlation (Pair corr.) of TREK-1 with A647 conjugated cholera toxin B (CTxB) was determined by two-color dSTORM and decreased with 3 dynes/cm^2 orbital fluid shear. (**b**) The same experiments as (a) is shown using pair correlation from the eGFP C-terminally expressed with TREK-1 instead of cy3b labeled anti-TREK-1 antibody. The eGFP in in dSTORM buffers produced a robust dSTORM signal. The data also provides a direct comparison of permeabilized cells vs. non-permeabilized seen Fig. 2b. Pair Corr. of TREK-1 with GM1 decreased dramatically decreased in three conditions. (**c**) A comparison of cy3b-STORM with eGFP-STORM seen in (Fig. 2e) in the presence of xPLD2. (**d-e**) A comparison of non-permeabilized (a) vs. permeabilized (b) HEK293T cells over expressing full length human TREK-1 and endogenous PLD2 (enPLD2), i.e., no over expression of PLD. (**f**) TREK-1/PIP$_2$ Pair correlation increased slightly after shear. The insets show, in a-d, the variability at a single radius. Statistics for single points were calculated with a student's t test. Statistical comparisons at multiple radii were made with a nested student's t test. (**g**) Schematic of brain slices mounted for dSTORM. Mouse brains fixed by whole body perfusion were sliced, labeled with cy3b-anti-TREK1 antibody and A647 CTxB and placed on a cover slip with fiberglass filter paper on top to hold the tissue in place during imaging. dSTORM buffer was added to the filter paper. The fluorescent background (640 nm) was undetectable at saturating intensities of light. (**h**) example images of brain slices from control and astrocyte specific SREBP2 null mice. TREK-1 was expressed in most areas of the brain, but not all (left panel). Pair correlation was determined from regions with both TREK-1 and CTxB labeling. The slice is coronal section near the hippocampus, but the exact region of interest is unknown.

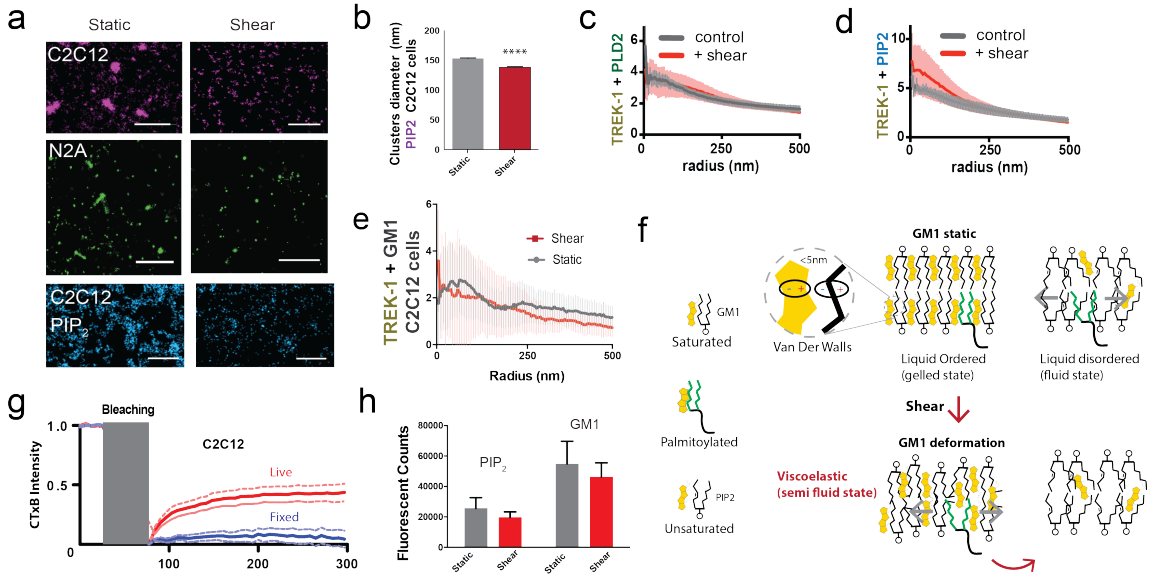

Supplemental Figure 5. **Observing cellular changes in response to mechanical stimulation**. (**a**) Representative images showing the effect of shear on the apparent size of GM1 (maroon and green) in C2C12 and N2a cells respectively. PIP_2 clusters in muscle C2C12 cells are shown in blue. When shear force is applied the apparent size decreases. Scale bars = 1 μm. (**b**) cluster analysis of PIP_2 show a small but significant decrease. (**c**) TREK-1 and PLD2 are complexed before and after shear in C2C12 cells. TREK-1 and PLD2 cross pair correlations are shown before (grey line) and after (red line) 3 dynes/cm^2 shear. Their association remains almost identical in both states. (**d**) TREK-1 staining with phosphatidylinositol 4,5 bisphosphate (PIP_2) antibody in C2C12 cells. Before shear (grey line) TREK-1 associated significantly with PIP_2, after shear the association further increased, suggesting some TREK-1 complex moved to PIP_2 clusters in C2C12 cells. (**e**) Shear pair correlation of TREK-1 with GM1 clusters (CTxB) measured by dSTORM in C2C12 cells prior to cholesterol loading showing in Fig. 4b. In low cholesterol endogenous TREK-1 clusters very little with GM1 lipids. (**f**) Shear thinning model for PLD2. Cholesterol is shown packing with saturated lipids and saturated palmitate via Van der Waals interaction (within 5 nm). Unsaturated lipids contain a double bond that changes to packing surface of a lipids. In a perfectly ordered state palmitoylated proteins are ordered with the GM1 lipids and cholesterol. In the disordered region palmitates are fluid within the membrane. After shear the GM1 lipids remain ordered but deformed. The palmitates no longer pack efficiently with the GM1 lipids, decreasing their affinity for the ordered domain and allowing the palmitates to move in the membrane. (**g**) Fluorescence recovery after photobleaching (FRAP) imaging to examine potential labeling artifacts[57,61,62] of pentavalent CTxB that could remain after fixation. The duration of bleaching is shown in grey. Blue line shows that PFA and glutaraldehyde fixation is sufficient to restrict the large-scale movement of lipids in fixed cells when compared to live cells (red). (**h**) For both PIP_2 and GM1 labeling, shear did not decrease the overall counts with dSTORM significantly in C2C12 cells ($p > 0.05$, Student's t-test).

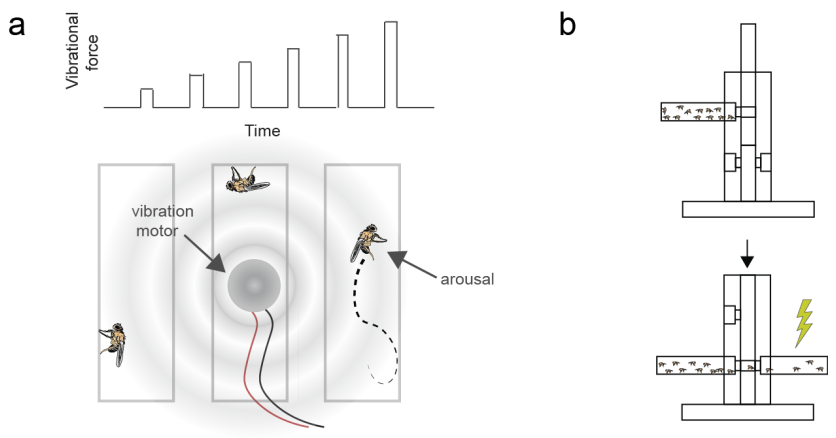

Supplemental Figure 6. **Pan-neuronal knockdown of *pld* in Drosophila results in a change in sensitivity to shock**. (**a**) PLD in N2a cells show an increase in activity when subjected to mechanical force. (**b**) Mechanical stimulation was applied in a series of six increasing vibrations (top). Vibration motor was attached to the back of the chamber with the flies and flies were monitored using a web camera for stimulation-induced arousal (bottom).

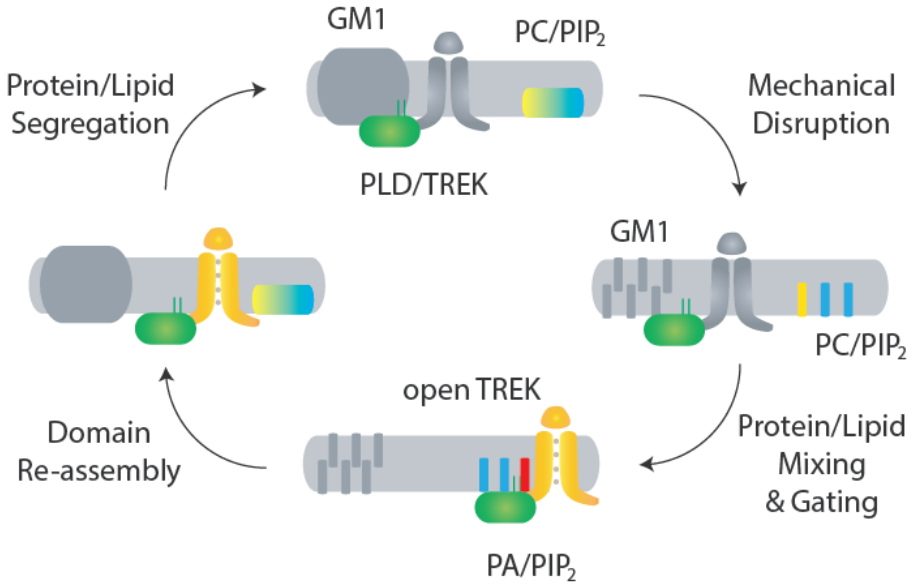

Supplemental Figure 7. **Proposed Lipid mixing model of TREK-1 mechanosensation**. In domain-mediated mechanosensation, in an unstimulated state, domains are intact, isolating the PLD2/TREK-1 complex from their respective activating lipids (PC/PIP_2, top). After stimulation, the raft is disrupted, causing the PLD2/TREK-1 complex to translocate (right) and eventually bind to PC and PIP_2. Upon binding, PLD2 is activated (bottom) transducing the mechanical signal to a chemical signal which then binds to and activates TREK-1 in chemical-to-electrical transduction. Upon stimulation removal, the domain reforms (left) causing the complex to be re-sequestered, causing a return to steady-state conditions (top).

Supplemental references

53. Brohawn, S. G., del Marmol, J., MacKinnon, R. & del Mármol, J. Crystal Structure of the Human K2P TRAAK, a Lipid- and Mechano-Sensitive K+ Ion Channel. *Science (80-.).* **335**, 436–441 (2012).

54. Su, Z., Brown, E. C., Wang, W. & MacKinnon, R. Novel cell-free high-throughput screening method for pharmacological tools targeting K+ channels. *Proc. Natl. Acad. Sci. U. S. A.* **113**, 1602815113-(2016).

55. Tanaka, K. A. K. *et al.* Membrane molecules mobile even after chemical fixation. *Nat. Methods* **7**, 865–866 (2010).

56. Veatch, S. L. *et al.* Correlation functions quantify super-resolution images and estimate apparent clustering due to over-counting. *PLoS One* **7**, (2012).

57. Moon, S. *et al.* Spectrally Resolved, Functional Super-Resolution Microscopy Reveals Nanoscale Compositional Heterogeneity in Live-Cell Membranes. *J. Am. Chem. Soc.* **139**, 10944–10947 (2017).

58. Lang, T. *et al.* SNAREs are concentrated in cholesterol-dependent clusters that define docking and fusion sites for exocytosis. *EMBO Journal* **20**, 2202–2213 (2001).

59. Coltharp, C., Yang, X. & Xiao, J. Quantitative analysis of single-molecule superresolution images. *Curr. Opin. Struct. Biol.* **28**, 112–121 (2014).

60. Devilliers, M. *et al.* Activation of TREK-1 by morphine results in analgesia without adverse side effects. *Nat. Commun.* **4**, 2941 (2013).

61. Raghunathan, K. & Kenworthy, A. K. Dynamic pattern generation in cell membranes: Current insights into membrane organization. *Biochim. Biophys. acta. Biomembr.* **1860**, 2018–2031 (2018).

62. Wang, H., Feng, Z., Del Signore, S. J., Rodal, A. A. & Xu, B. Active Probes for Imaging Membrane Dynamics of Live Cells with High Spatial and Temporal Resolution over Extended Time Scales and Areas. *J. Am. Chem. Soc.* **140**, 3505–3509 (2018).